Ozone source apportionment during peak summer events over southwestern Europe

María Teresa Pay[1], Gotzon Gangoiti[2], Marc Guevara[1], Sergey Napelenok[3], Xavier Querol[4], Oriol Jorba[1], Carlos Pérez García-Pando[1]

[1]Earth Sciences Department, Barcelona Supercomputing Center, BSC, c/Jordi Girona, 29, 08034 Barcelona, Spain
[2]Department of Chemical and Environmental Engineering, University of the Basque Country UPV/EHU, ETSI-Bilbao School of Engineering, Alda. de Urquijo s/n, E-48013 Bilbao, Spain.
[3]U.S. EPA, Research Triangle Park, NC, USA.
[4]Institute of Environmental Assessment and Water Research, IDAEA-CSIC, c/Jordi Girona, 18-26, 08034 Barcelona, Spain.

Correspondence to: María Teresa Pay (maria.pay@bsc.es)

Abstract. It is well established that in Europe, high O_3 concentrations are most pronounced in southern/Mediterranean countries due to the more favorable climatological conditions for its formation. However, the contribution of the different sources of precursors to O_3 formation within each country relative to the imported (regional and hemispheric) O_3 is poorly quantified. This lack of quantitative knowledge prevents local authorities from effectively designing plans that reduce the exceedances of the O_3 Target Value set by the European Air Quality Directive. O_3 source attribution is a challenge because the concentration at each location and time results not only from local biogenic and anthropogenic precursors, but also from the transport of O_3 and precursors from neighbouring regions, O_3 regional and hemispheric transport and stratospheric O_3 injections. Our study applies and thoroughly evaluates a countrywide O_3 source apportionment method implemented in a Chemical Transport Model (CTM) at high resolution (4 x 4 km) over the Iberian Peninsula (IP) to understand and quantify the origin of peak O_3 events over a 10-day period covering the most frequent synoptic summer conditions in the IP. The method tags both O_3 and its gas precursor emissions from source sectors within one simulation and each tagged species is subject to the typical physical processes (advection, vertical mixing, deposition, emission and chemistry) as the actual conditions remain unperturbed. We quantify the individual contributions of the largest NO_x local sources to high O_3 concentrations compared to the contribution of imported O_3. We show for the first time that imported O_3 is the largest input to the ground-level O_3 concentration in the IP, accounting for 46% to 68 % of the daily mean O_3 concentration during exceedances of the European Target Value. The hourly imported O_3 increases during typical northwestern advections (70-90%, 60-80 µg/m³), and decreases during typical stagnant conditions (30-40%, 30-60 µg/m³) due to the local NO titration effect. During stagnant conditions, the anthropogenic precursors control the O_3 peaks in areas downwind of the main urban and industrial regions (up to 40% in hourly peaks). We also show that ground-level O_3 concentrations are strongly affected by vertical mixing of O_3-rich layers present in the free troposphere, which result from local/regional layering and accumulation, and continental/hemispheric transport. Indeed, vertical mixing largely explains the presence of imported O_3 at ground level in the Iberian Peninsula. Our results demonstrate the need for detailed quantification of the local and remote

Atmospheric
Chemistry
and Physics
Discussions

contributions to high O_3 concentrations for local O_3 management, being the O_3 source apportionment an essential analysis prior to the design of O_3 mitigation plans in any non-attainment area. To achieve the European O_3 objectives in southern Europe, *ad hoc* local actions should be complemented by decided national and European-wide strategies.

1 Introduction

5   Tropospheric ozone (O_3) is an air pollutant of major public concern as it harms human health (WHO, 2013) and sensitive vegetation (Booker et al., 2009), and contributes to climate change (Jacob and Winner, 2009). O_3 is formed in the atmosphere through nonlinear photochemical reactions among carbon monoxide (CO), peroxy radicals generated by the photochemical oxidation of volatile organic compounds (VOC), and nitrogen oxides (NO_x) (Crutzen, 1973). Therefore, meteorological stagnation, high temperature, and low precipitation enhance tropospheric O_3 formation (Demuzere et al.,
10 2009; Otero et al., 2016). Atmospheric circulation also controls the short and long-range transport of O_3 affecting its lifetime in the atmosphere (Monks et al., 2015). For example, the transport of precursors emitted in urban and industrialized areas may cause O_3 production downwind (Holloway et al., 2003).

According to the European Environmental Agency (EEA) around 95-98% of the population in Europe during 2013-2015
15 were exposed to O_3 concentrations that exceeded the guidelines of the World Health Organization (WHO) (EEA, 2017). These guidelines establish a maximum daily 8-hour averaged (MDA8) O_3 concentration of 100 μgm^{-3} never to be exceeded. The European Air Quality Directive (2008/50/EC) is less restrictive as it sets an O_3 Target Value of 120 μgm^{-3} for the MDA8 concentration, which can be exceeded up to 25 days per calendar year averaged over three years.

20 Southern European countries around the Mediterranean Basin are particularly exposed to exceedances of the O_3 Target Value in summer due to the influence of frequent anticyclonic and clear-sky conditions that favour photochemical O_3 formation in the troposphere (EEA, 2017). In addition, its geographic location also makes the Basin a receptor of the long-range transport of pollution from Europe, Asia and even North America (Lelieveld et al., 2002; Gerasopoulos, 2005). The importance of long-range transport on surface O_3 has been studied in the Mediterranean Basin, indicating that the emission
25 sources within the Basin have a dominating influence on surface O_3, while remote sources are more important than local sources for O_3 mixing ratios at higher altitudes (Richards et al., 2013; Safieddine et al., 2014). Recent studies suggest that the upper O_3-rich air masses could increase the surface O_3 concentration in the Mediterranean Basin (Kalabokas et al., 2017; Querol et al., 2018). Further detailed and quantitative studies on the mechanism linking upper O_3-rich layer with increases of the ground-level O_3 concentration in episodes need further clarification particularly regarding the contribution of O_3
30 transported at regional and hemispheric scales.

Atmospheric
Chemistry
and Physics
Discussions

Several studies in the Iberian Peninsula have addressed the causes of O_3 episodes looking at the circulation of air masses (Millán, 2014, and references therein). In the Atlantic region, the blocking anticyclones over Western Europe favour the inter-regional transport of O_3 in the area and its accumulation for several days during the most severe episodes (Alonso et al., 2000; Gangoiti et al., 2002, 2006; Valdenebro et al., 2011; Saavedra et al., 2012). On the other hand, in the Mediterranean

5   coast, the typical summer synoptic meteorological conditions with a lack of strong synoptic advection, combined with the orographic characteristics and the sea and land breezes, favour episodes where high levels of O_3 are accumulated by recirculation of air masses loaded with O_3 precursors (Millán et al., 1997 and 2000; Toll and Baldasano, 2000; Gangoiti et al., 2001; Pérez et al., 2004; Jiménez et al., 2006; Gonçalves et al., 2009; Millán, 2014, Querol et al., 2017; Querol et al., 2018). The coupling between synoptic and mesoscale processes governing the levels of O_3 in the Western Mediterranean

10   Basin need further research in order to understand the O_3 intercontinental contribution. Furthermore, from our understanding there is a lack of research quantifying the contribution of the activity sources to the O_3 local formation during peak events in this region.

O_3 analyses in the Western Mediterranean Basis show that regional background O_3 levels have remained high without

15   significant changes (EEA, 2016; EMEP-CCC, 2016; Querol et al., 2016). However, they have increased at traffic and urban background sites (EEA, 2016; Querol et al., 2016; Sicard et al., 2016; Saiz-Lopez et al., 2017). The reasons behind the urban O_3 upward trend are not clear yet; it might be a result of the reduction of NO emissions relative to NO_2 and therefore a lower NO titration effect or the fact that urban O_3 formation is VOC-limited, and a reduction in NO_x emissions might enhance O_3 formation. The most intense O_3 events in the last decade, measured by the number of exceedances of the O_3 Target Value are

20   recorded over areas downwind of large urban and industrial hot spots (Monterio et al, 2012; Querol et al., 2016; EEA, 2016). Overall, the number of these type O_3 events occur in June-July and during summer heatwaves (i.e., 2003 and 2015).

According to the European Air Quality Directive, in zones exceeding the O_3 Target Value, Member States must develop plans to attain compliance by reducing the emission of O_3 precursors. Abatement of tropospheric O_3 concentration in the

25   Western Mediterranean Basin has been insufficient so far (Querol et al., 2018). Effective planning requires an accurate quantitative knowledge of the sources of these precursors and their respective contributions to the exceedances of the O_3 Target Value (Querol et al., 2016; Borrego et al., 2015). However, source attribution of surface O_3 concentration remains a challenge, because the concentration at each location and time results not only from local biogenic and anthropogenic precursors, but also from the transport of O_3 and its precursors from neighbouring regions, O_3 hemispheric transport

30   (UNECE, 2010), and stratospheric O_3 injections (Monks et al., 2015).

At present, there are no methods based on observations that distinguish the origin of O_3. Despite their inherent uncertainties, Chemical Transport Models (CTMs) allow apportioning the contribution of any source (by sector and/or region) to O_3 concentrations. The most widely used approach is the "brute force" method, which consists on running an ensemble of

simulations zeroing out the sources one by one and then comparing them with a baseline simulation that accounts for all of the sources. Several O_3 source apportionment studies at European scale have applied the brute force method to quantify the contribution of one or two emission sectors. For example, road transport emissions with the EMEP model (Reis et al., 2000), biogenic and anthropogenic emissions with the Polyphemus model (Sartelet et al. 2012), transport-related emissions

5 including road transport, shipping, and aviation with the WRF-CMAQ model (TRANSPHORM, 2014), and ship emissions with CAMx (Aksoyuglu et al., 2016). This approach is simple to implement, as it does not require additional coding in the CTM. However, as it quantifies the contribution of each source based on its absence, it does not reproduce actual atmospheric conditions, and therefore it is susceptible to inaccuracies in the prediction of O_3 peaks under non-linear regimes (Cohan and Napelenok, 2011). Despite these limitations, brute force is useful for analysing the concentration responses to

10 emission abatement scenarios.

Recently, CTMs include algorithms that tag multiple pollutants by source (region and/or sector) all the way through the pollutant's lifetime, from emission to deposition. This integrated source apportionment approach has several advantages. First, it allows identifying the main sources contributing to high O_3 levels under actual atmospheric conditions, which is a

15 preliminary step towards designing refined and efficient emission abatement scenarios. Second, as we show below, it supports enhanced model evaluation and therefore potential model improvements by identifying problems in emission estimates (sectors or regions) or chemical boundary conditions. The Integrated Source Apportionment Method (ISAM) within the Community Multiscale Air Quality (CMAQ) model has shown promising results for O_3 tagging, exhibiting less noise in locations where brute force results are demonstrably inaccurate (Kwok et al., 2013, 2015). Recent ISAM

20 experiments have quantified that the contribution of traffic in the cities of Madrid and Barcelona to the daily O_3 peaks downwind of the urban areas is particularly significant (up to 80-100 μgm^{-3}) (Valverde et al., 2016a). O_3 tagging methods are also included in other regional and global models applied over Europe (Karamchandani et al., 2017; Butler et al., 2018).

The integrated source apportionment tools combined with high-resolution emission and meteorological models can help

25 unravelling the sources responsible for peak summer events of O_3 in the Western Mediterranean Basin. Quantifying the contribution of emission sources during acute O_3 episodes is a prerequisite for the design of future mitigation strategies in the region. Our study applies for the first time a countrywide O_3 source apportionment at high resolution over the Iberian Peninsula to investigate the local sources responsible for high O_3 concentration compared to the imported (regional and hemispheric) O_3 during a typical summer episode. Our analysis focuses on the period between July 21st and 31st, 2012, which

30 is representative of the typical summer synoptic conditions in the region. We use the CMAQ-ISAM within the CALIOPE air quality forecast system for Spain (www.bsc.es/caliope), which runs at 4-km horizontal resolution over the IP. The system is fed by the HERMESv2.0 emission model, which provides disaggregated emissions based on local information and state-of-the-art bottom-up approaches for the most polluting sectors.

Atmospheric
Chemistry
and Physics
Discussions

Open Access

EGU

The paper is organized as follows. In Section 2 we introduce the CALIOPE system, the set-up of ISAM and the HERMESv2.0 emission model for O_3 source apportionment studies, and the methodology used to quantify evaluate the model. In Section 3 we demonstrate the representativeness of the selected episode, we evaluate the model, and we provide an analysis of the source-sector contribution to the Spanish O_3 under the different synoptic patterns occurring during the study

5   period. In Section 4, we discuss our findings, the regulatory implications, and future research.

2 Methodology

2.1 Air quality model

We used the CALIOPE air quality modelling system (www.bsc.es/caliope) to simulate the O_3 dynamics over the IP during the selected episode. CALIOPE is described elsewhere (Baldasano et al., 2008; Pay et al., 2014; Valverde et al., 2016a; and

10   reference therein). The system consists of the HERMESv2.0 emission model (Guevara et al, 2013), the WRF-ARWv3.6 meteorological model (Skamarock and Klemp, 2008), the CMAQ v5.0.2 chemical transport model (Byun and Schere, 2006) and the BSC-DREAM8bv2 mineral dust model (Basart et al., 2012). CALIOPE first runs over Europe at 12-km resolution (EU12 domain) and then over the IP at 4-km (IP4 domain) (Fig. S1). In the present work, the system is configured with 38 sigma layers up to 50 hPa, both for WRF and CMAQ. The planetary boundary layer is characterized with approximately 11

15   layers, where the bottom layer's depth is ~39 m. The EU12 domain uses meteorological initial and boundary conditions from the Final Analyses provided by the National Centers of Environmental Prediction (FNL/NCEP) at 0.5º by 0.5º. The first 12 h of each meteorological run are treated as cold start, and the next 23 h are provided to the chemical transport model. Boundary conditions for reactive gases and aerosols come from the global MOZART-4/GEOS-5 model at 1.9º by 2.5º (Emmons et al., 2010). CMAQ uses the CB05 gas-phase mechanism with active chlorine chemistry, an updated toluene

20   mechanism (CB05TUCL; Whitten et al., 2010; Sarwar et al., 2012), and the sixth generation CMAQ aerosol mechanism including sea salt, aqueous/cloud chemistry and the ISORROPIA II thermodynamic equilibrium module (AERO6; Reff et al., 2009; Appel et al., 2013). Table S1 depicts the remaining CALIOPE configuration options.

For the IP4 domain, HERMESv2.0 estimates emissions for Spain with a temporal and spatial resolution of 1 h and up to 1

25   km by 1 km, according to the Selected Nomenclature for Air Pollution (SNAP), which are then aggregated to 4 km resolution (Guevara et al., 2013). HERMESv2.0 is currently based on 2009 data, which is the most recent year with updated information on local emission activities. For neighbouring countries and international shipping activities, HERMESv2.0 uses the annual gridded national emission inventory provided by the European Monitoring and Evaluation Programme (EMEP) disaggregated to 4 km resolution using a SNAP-sector-dependent spatial, temporal and speciation treatment (Ferreira et al.,

30   2013). The VOC and NO_x emissions from vegetation, which are critical in the formation of O_3, are estimated with the Model of Emissions of Gas and Aerosols from Nature (MEGANv2.0.4) (Guenther et al., 2006) using temperature and solar

radiation from the WRF model. HERMESv2.0 is suitable for source apportionment studies thanks to its level of detail in the calculation of the emission fluxes by source (Guevara et al., 2014).

2.2 Ozone source apportionment method

We applied ISAM to quantify contributions from different SNAP categories to the surface O_3 over the IP. The ISAM O_3
5   tagging method is a mass balance technique that tags both O_3 and its gas precursor emissions (NO_x and VOC) from each source sector within one simulation (Kwok et al., 2013, 2015). Each tagged species undertakes typical physical processes (advection, vertical mixing, deposition, emission and chemistry) without perturbing the actual conditions. The O_3 rate of change for each tag in any grid cell is calculated as follows (Eq. 1):

$$\frac{dc_{tag}}{dt} = P_{tag} - D \frac{c_{tag}}{\Sigma_{tag} c},$$ (1)

10

Where C_{tag} represents the O_3 concentration related to a tagged source of interest, P_{tag} is the chemical production rate of O_3 formed by the precursors emitted for each tag, and D is the total chemical destruction rate of O_3 in this grid cell. Different ratios of NO_x/VOC cause the formation of O_3 in each grid cell, which is controlled either by NO_x- or VOC-limited conditions. ISAM uses the ratio H_2O_2/HNO_3 to determine whether O_3 is NO_x- or VOC-sensitive (above or below 0.35,
15   respectively) (Zhang et al., 2009). The bulk O_3 concentration in each model grid cell (P_{bulk}) is equal to the sum of O_3 tracers that were produced in either NO_x or VOC-sensitive conditions (Eq. 2),

$$P_{bulk} = \Sigma_{tag} P_{tag} = \Sigma_{tag} P_{tag}^N + \Sigma_{tag} P_{tag}^V,$$ (2)

20   where P_{tag}^N and P_{tag}^V are the O_3 produced under NO_x- and VOC-limited conditions, respectively according Eqs. 3 and 4:

$$P_{tag}^{N,new} = P_{tag}^{N,old} + P_{bulk}^{new} \frac{\Sigma_x NO_{x,tag}}{\Sigma_{tag} \Sigma_x NO_{x,tag}},$$ (3)

$$P_{tag}^{V,new} = P_{tag}^{V,old} + P_{bulk}^{new} \frac{\Sigma_y VOC_{y,tag} \times MIR_y}{\Sigma_{tag} \Sigma_y VOC_{y,tag} \times MIR_y},$$ (4)

$NO_{x,tag}$ and $VOC_{j,tag}$ are the concentrations of the x nitrogen and y VOC species in CB05 that participate in the photochemical
25   O_3 formation for each source sector tag and grid cell. MIR_y is the maximum incremental reactivity factor of each y species of VOC emitted by each source sector tag, corresponding to the O_3 generating potential of each single VOC species (Carter, 1994).

2.3 Ozone tagged species

Table 1 summarizes the O_3 tagged sources in the present study and Fig. 1a depicts the HERMESv2.0's estimates of the contribution by each SNAP category to the total emissions of O_3 precursors in Spain. The largest NO_x sources are road transport (SNAP7; 42%), non-road transport (SNAP8; 19%), manufacturing industries (SNAP34; 16%), and energy

5   production (SNAP1; 16%). VOC are dominated by biogenic sources (SNAP11; 70%) and to a lesser extent by the agricultural sector (SNAP10; 11%), solvent and other product uses (SNAP6; 9%) and road transport (SNAP7; <7%). The selected (tagged) SNAP categories in this study are the energy, industrial, road transport and non-road transport sectors (Fig. 1b), which account for the 92% of the total NO_x emissions in Spain. An additional tracer (OTHR) gathers the remaining emission categories that were not explicitly tracked (i.e., SNAP2, 5, 6, 9, 10 and 11).

10

In addition to the selected sources, we tracked the contributions of the chemical boundary conditions (BCON) and the initial conditions (ICON). BCON represents both the O_3 directly transported through the IP4 domain boundaries and the formation of O_3 resulting from precursors that are also transported through the boundaries. BCON O_3 comes from the EU12 parent domain, which includes the O_3 produced in Europe and the O_3 transported at global scale (both tropospheric and

15   stratospheric O_3) provided by the MOZART-4/GEOS model (Fig. S1). Hereinafter, we name BCON O_3 as the imported O_3 to the IP4 domain. Tagging the O_3 initial allows quantifying the number of spin-up days to minimize the impact of model initialization. For the present run, we required 6 days of spin-up to set the contribution of initial conditions to less than 1% of the net hourly O_3 concentration over 95% of the available O_3 stations.

2.4 Evaluation method

20   We evaluate the simulated concentrations against air quality measurements from the Spanish monitoring stations that are part of the European Environment Information and Observation Network (EIONET; https://www.eionet.europa.eu/). The EIONET network provides a relatively dense geographical coverage of the Spanish territory. During the July 21st-31st episode we used the measurements from 347 stations for O_3 and 357 stations for NO_2 with a temporal coverage above 85% on an hourly basis. Fig. S2 shows the distribution of the stations for O_3 and NO_2.

25

The evaluation based on discrete statistics includes the correlation coefficient (r), Mean Bias (MB), and the Root Mean Square Error (RMSE) (Appendix B). We used the package "openair" (Carslaw and Ropkins, 2012) for R (v3.3.2; R Core Team, 2016) to compute the statistics. We calculate statistics on an hourly basis for O_3 and NO_2, as well as for the regulatory MDA8 in the case of O_3. The evaluation also takes into account the station type, following the categories established by the

30   EEA (i.e., rural background, urban background, industrial and traffic).

There are no direct evaluation methods for apportioned pollutants. Instead, we designed a diagnostic plot for source apportionment analysis at each individual receptor, including a time series of measured and observed O_3 and NO_2 concentrations together with the simulated tagged sources. In addition, this plot includes the simulated wind speed and direction. These plots are helpful as they compare the modelled O_3 and NO_2 with the observations, while highlighting the

5   sources and circulation patterns at least partly responsible for the model behaviour. This work will only discuss in detail the source apportionment plots at key O_3 receptor regions, given the high number of stations (260) that simultaneously measure O_3 and NO_2.

3 Results

3.1 Description of the ozone episode

10   In 2012, the largest O_3 episode in Europe occurred between July 21st and 31st. That period alone comprised 33% of the total number of exceedances of the information threshold, and 12% of the number of exceedances of the O_3 Target Value in 2012 (EEA, 2013). In Spain, around 60% of the annual exceedances also occurred during this period. (As shown in Querol et al. (2016) July is typically the month with the highest number of O_3 exceedances in Spain.) The episode affected the central and north of the IP (Fig. 2c), in particular the 90th percentile of the MDA8 O_3 concentration exceeded the Target Value at the

15   surroundings of the Madrid Metropolitan Area (MMA), and an area located north of the Barcelona Metropolitan Area (BMA), which correspond to hotspots and the tail end of large urban and/or industrial plumes.

Figure 2a shows the observed MDA8 O_3 concentrations trends at the Spanish EIONET stations during the (extended) summers (i.e., from April to September) from 2000 to 2012, together with the values recorded during the selected episode.

20   We have categorized the MDA8 O_3 concentrations by station type. Rural background stations show the highest MDA8 O_3 concentrations during the episode followed by industrial, traffic and urban stations, which is consistent with the observed previous summer patterns. More specifically, the episode shares a similar 75th percentile (75p) of the MDA8 O_3 concentrations at rural background stations above the Target Value with the particularly severe summer of 2003 (Solberg et al., 2008). Note that the MDA8 O_3 concentrations at rural and urban background sites barely changed between 2000 and

25   2012, which suggests that the benefits from European emission controls may have been significantly counterbalanced by increasing background O_3 (Monks et al., 2015). In contrast, the MDA8 O_3 concentrations at TR and IN sites slightly increased, likely because of a lower O_3 titration due to the preferential abatement of NO vs. NO_2. However, we need more research on O_3 source apportionment to confirm this hypothesis (Querol et al., 2016; Sicard, et al., 2016).

30   Figure 2b shows the number of observed exceedances of the O_3 Target Value per day during the selected episode. There were more than 100 exceedances in most of the days, with relative maxima on July 25th, 28th and 31st attributed to the change in the synoptic conditions. Figure 3 shows the meteorological patterns (2m temperature, 10m wind, precipitation, mean sea

Atmospheric
Chemistry
and Physics
Discussions

level pressure and geopotential height at 500 hPa) modelled by WRF-ARW during the three distinctive days over the outer EU12 domain.

Stagnant conditions and northwestern advections are the most frequent summer synoptic circulation patterns over the IP, occurring ~44% of the days in a year (Jorba et al., 2004; Valverde et al., 2014). Stagnant conditions are characterized by reduced surface pressure gradients and weak synoptic winds, intense solar radiation, and the development of the Iberian Thermal Low (ITL). The ITL forces the convergence of surface winds from the coastal areas towards the central plateau enhancing sea breezes and mountain-valley winds and subsidence over the Western Mediterranean Basin as described by (Millán et al., 1997, 2000; Millán 2014). In contrast, northwestern advections (NWad) transport air masses from the Atlantic towards the north and west of the IP and they are characterized by atmospheric instability and intense ventilation. Periods of accumulation and venting of pollutants follow the same sequence of pressure ridging and throughing respectively, of the lower and middle troposphere of the IP during the warm season (Querol et al., 2017). The selected episode started with the development of an accumulation- ITL period (July 21st-25th), followed by a NWad-venting period (July 26th-29th) and ended with the development of another ITL (July 30th-31st).

Figure 4 shows the 90th percentile (90p) of the simulated hourly O_3 and NO_2 concentrations corresponding to the three distinctive days with the relative maxima of exceedances. In the northern Spanish Mediterranean areas, intense O_3 episodes often affect the plains and valleys located to the north of the BMA in summer (Toll and Baldasano, 2000; Gonçalves et al., 2009; Valverde et al., 2016a; Querol et al., 2017). High NO_x concentrations from the BMA combined with high summer biogenic VOC levels are driven inland by sea breezes and mountain valley winds, channelled by north-south valleys towards an intra-mountain plains located 60 km north of the BMA. This happened on July 31st when the highest 90p of the hourly O_3 concentrations (160-180 µgm^{-3}) in Spain occurred over N and NW BMA. Occasionally, as it happened on July 25th, anticyclonic winds over the western Mediterranean Sea deflect the sea-breeze flow enriched with precursors from the BMA towards the Gulf of Lion where it reaches the highest 90p of the hourly O_3 concentrations (160-180 µgm^{-3}) in the IP Mediterranean region. Eastern Spanish Mediterranean areas show similar O_3 dynamics, with inland regions depicting the highest O_3 peaks (140-160 µgm^{-3}) when low-pressure gradients cover central and eastern IP.

In the centre of the IP intense O_3 episodes occurred during the development of the ITL, where the affected area depends on the synoptic conditions. Under the absence of synoptic forcing (e.g., July 25th), the MMA had the highest 90p of the hourly O_3 concentrations (~140-160 µgm^{-3}). In contrast, when mountain valley winds are reinforced with synoptic westerlies (e.g., July 31st) (Fig. 3) the urban NO_x plume is channelled along the mountain ranges in Madrid towards the northeast and the highest 90p of the hourly O_3 concentrations are found along the valley (~140-160 µgm^{-3}).

Atmospheric
Chemistry
and Physics
Discussions

In the northern and northeastern of the IP, the 90p of the hourly O_3 concentrations show a significant increase when the blocking anticyclone over Western Europe is combined with the development of the ITL (e.g. July 25th). The stagnant conditions favour the accumulation of O_3 precursors around main cities and industrial areas and enhance the local O_3 formation.

5

The NWad pattern (e.g., July 28th) significantly decreases the 90p of the hourly O_3 concentrations in the central and northern IP. The northwesterly winds decrease the temperature and therefore the O_3 formation. As consequence, O_3 levels are reduced in the plumes from the BMA and the MMA, although they are still significant in the latter. Overall, the 90p of the hourly O_3 concentrations during the NWadv pattern were ~100 μgm^{-3} in most background areas. In contrast, during the ITL it was
10   above 120 μgm^{-3}.

3.2 Statistical evaluation

CALIOPE has been evaluated in detail elsewhere (Pay et al., 2014 and references therein). Here, we evaluate the updated version of CALIOPE using ISAM to quantify the system's ability to reproduce O_3 and NO_2 concentrations. Table 2 compiles the quartiles of the statistics calculated by station type. (Note that there are stations not fitting any of the four categories (i.e.,
15   IN, TR, UB and RB), so the exceedance/station numbers in the IN/TR/UB/RB rows do not sum up to the numbers in the "ALL" rows.)

The model slightly overestimates the hourly and MDA8 O_3 concentrations with MB of +12 μgm^{-3} and +6 μgm^{-3}, respectively. The r is above 0.6 in more than 50% of the stations and above 0.7 in 25% of them. The MB for hourly and
20   MDA8 O_3 concentrations are lower at RB stations (±4 μgm^{-3}) than at IN, TR and UB stations (between +6 and +16 μgm^{-3}) in 50% of the stations. As expected, the highest number of exceedances of the O_3 Target Value was recorded at RB stations (260 exceedances) followed by IN stations (204 exceedances).

At RB stations, hourly O_3 is overestimated (+4 μgm^{-3}) and MDA8 O_3 is underestimated (-4 μgm^{-3}), which indicates that
25   nighttime O_3 is overestimated. The nighttime overestimation is a common feature of CTMs and it is typically attributed to the underestimation of vertical mixing during nighttime stable conditions and to underestimation of the O_3 titration by NO (Bessagnet et al., 2016; Sharma et al., 2017).

CALIOPE underestimates the hourly NO_2 concentrations with -7 μgm^{-3} at TR stations and -2 μgm^{-3} at RB stations. This
30   partly explains the high overestimation of the hourly and MDA8 O_3 concentration at TR and UB stations, as well as the systematic overestimation of hourly O_3 concentration at nighttime (due to a lack of O_3 titration by NO). The hourly NO_2 concentration at TR stations feature the highest r (with 25% of stations above 0.6), which proves the reasonably accurate representation of temporal emission in urban areas by the HERMESv2.0 (Guevara et al, 2014; Baldasano et al., 2011). In

Atmospheric
Chemistry
and Physics
Discussions

contrast, the RMSE is highest at TR stations, which results from the underestimation of NO_2 peaks during traffic rush hours. Underestimation of NO_2 traffic peaks is a common problem in Eulerian mesoscale models (Pay et al., 2014), as emission heterogeneity is lost in the grid cell-averaging process, which is especially critical in urban areas. Next generation microscale models will potentially solve this problem (Lateb et al., 2016). Besides the dilution of the emission in the grid, meteorology

5 also may play an important role in the low performance of NO_2 and O_3 in hotspot areas. Several inter-comparison studies (e.g., EURODELTA and AQMEII) agree on the limitations of models to simulate meteorological variables that affect the hourly NO_2 temporal variability, which controls model performance for O_3 in high NO_x environments and areas downwind (Bessagnet et al., 2016; Solazzo et al., 2017).

10 Figure 5 classifies the hourly and MDA8 O_3 concentrations at the air quality stations into four MB categories that account for the 93% of stations. There are two categories with the lowest hourly O_3 MB (± 10 μgm^{-3}): type A with a MDA8 O_3 MB between -40 and -10 μgm^{-3} and type B with MDA8 O_3 MB of ± 10 μgm^{-3}. There are two categories with the highest hourly O_3 MB (between 10 and 40 μgm^{-3}): type C with a MDA8 O_3 MB of ± 10 μgm^{-3} and the type D with MDA8 O_3 MB between 10 and 40 μgm^{-3}. In addition, Fig. S2 depicts the MB, RMSE and r for hourly and MDA8 O_3, and hourly NO_2

15 concentrations. The best performances for O_3 (type B) are found at the 28% of the stations, located in the surroundings of the MMA, the BMA and most of the northern Mediterranean stations, which is consistent with the highest r ($0.6 < r < 0.9$) found in the center and north of the IP (Fig S3). The highest O_3 overestimations (type D) are present at 36% of the stations, mainly located in highly industrialized areas in Spain (Guadalquivir Basin, Strait of Gibraltar, Valencia) and inside the MMA. Next sections analyze the origin of these O_3 biases using the source apportionment time series.

20

The comparison with previous CALIOPE studies (Baldasano et al., 2011; Pay et al., 2014) indicates that r is in the same range for O_3 (0.6-0.7) and NO_2 (0.4-0.5) at individual stations; the same applies to RMSE (15-29 μgO_3 m^{-3} and 10-20 μgNO_2 m^{-3}). Modelled O_3 shows higher performance at traffic stations in large cities, since stations influenced by road transport emissions (i.e., high-NO_x environments) are better characterized with a more pronounced daily variability (Baldasano et al.,

25 2011).

3.3 Source-sector ozone contributions during peak episodes

Figure 6 shows the 90p of the hourly O_3 concentration over the IP tagged by source type (Table 1) for different days (July 25th, 28th and 31st). (Fig. S3 in the supplementary material shows similar plots for NO_2.) The imported O_3 is by far the largest contributor showing a 90p ranging from 70 to 120 μgm^{-3} in the east/north/centre of the IP on July 25th /28th /31st ,

30 respectively (Fig. 6). The imported O_3 enters the study domain through the IP4 domain boundaries and it can only be transported, scavenged deposited or depleted by O_3 precursors. Therefore, areas with low imported O_3 concentrations (< 50 μgm^{-3}) are good indicators of (1) the accumulation of specific O_3 precursors that deplete imported O_3, and (2) the subsequent O_3 photochemical production that occur mostly under stagnant conditions and around the largest industrial/urban areas. The

90p of the hourly imported O_3 concentration shows the lowest values in two different conditions and regions. First, on July 25th in the northwestern IP and Portugal, extremely low winds allow the accumulation of local pollutants that titrate imported O_3 concentrations down to 30-70 µgm^{-3}; at the same time O_3 is locally produced due to traffic emission downwind of major northern cities (La Coruña, Gijón, Bilbao) (60-120 µgm^{-3}), shipping activities (up to 40 µgm^{-3}) and the generation of energy and industrial processes (10-20 µgm^{-3}). Second, on July 31st in the northeastern IP, when the pollutants transported from the Gulf of Lion and Catalonia towards the Mediterranean act as a sink of imported O_3 reducing its concentration down to 60 µgm^{-3}. As a result, there is a local O_3 formation up to 120-160 µgm^{-3} along the Ebro Valley and the Lleida Plain.

After the imported O_3, the largest contributor to O_3 is the road transport sector. Downwind of the major urban areas in Spain (i.e., Madrid, Barcelona, Bilbao, Sevilla, Valencia, Gijon, Pontevedra), on-road traffic contributed to the 90p of the hourly O_3 concentrations as much as 60-120 µgm^{-3}, and affected different areas depending on the synoptic/mesoscale regimes (Fig. 6). In the northern BMA, the 90p of the hourly O_3 concentration from the road transport sector reaches its maximum when the stagnant conditions affects the centre and eastern IP (e.g., July 31st). As noted above, mesoscale winds carry traffic O_3 precursors from the BMA inland, channelled by north-south valleys towards the intra-mountain plain in the north. Over the MMA, the 90p of the hourly O_3 concentration from the road transport sector showed the maximum when the ITL was combined with the synoptic westerlies (e.g., July 31st), carrying high O_3 as far as to the Ebro Valley, as shown in Fig 4.

Regarding the contribution from the non-road transport sector, the Atlantic regions of the IP show the highest 90p of the hourly O_3 concentration (25-40 µgm^{-3}) on July 25th. The stagnant condition favoured the accumulation of precursors from the Atlantic shipping route and the formation of O_3 within the region. The Spanish Mediterranean region shows the highest 90p of the hourly O_3 concentrations from the non-road transport sector in front of the southeastern coasts of the IP (~180 µgm^{-3}) when the westerlies in the Strait of Gibraltar injected precursors from international shipping into the Mediterranean Basin (e.g., July 28th and 31st). Note that during days with high 90p of the hourly O_3 concentration from non-road transport, the imported O_3 concentration shows the lowest 90p due to the NO titration effect over emission areas.

The elevated point source emission sectors (i.e., energy and industry) contributed less to O_3 than the traffic sector, but their contributions were significant reaching 15-25 µgm^{-3} of the 90p of the hourly O_3 concentrations (Fig. 6). The north and northeastern IP, the Mediterranean coast, and the Guadalquivir Valley are the most affected regions under stagnant conditions.

The contribution of the remaining sectors (OTHR) to the 90p of the hourly O_3 concentrations was similar to that of the elevated point sources (15-25 µgm^{-3}), but it reached up to 30 µgm^{-3} in areas downwind of Oporto and Lisbon (Fig. 6). OTHR includes the formation of O_3 from the remaining anthropogenic and biogenic sources (accounting for less than 8% of total NO_x emissions, but 93% of total VOC). The high OTHR concentration around the biggest cities in Portugal may be related

to precursors emitted by the residential sector (SNAP2 and 9) and biogenic emissions, as found in other source apportionment studies over Portugal (Borrego et al., 2016; Karamchandani et al., 2017).

3.4 Regionalization of source-sector contributions

The analysis of the source-sector contributions to O_3 allowed identifying ten receptor regions with similar characteristics in terms of meteorological and O_3 patterns, main source contributors and geographical patterns (Figs. 4 and 6). Figure 7c shows the location of the air quality stations belonging to each receptor region corresponding to the central IP (CIP), the eastern IP (EIP), the Ebro Valley (EV), the Guadalquivir Valley (GV), the Mediterranean Sea (MED), the northeastern IP (NEIP), the northern IP (NIP), the northwestern IP (NWIP), the southern IP (SIP) and the western IP (WIP). The O_3 receptor regions are consistent with Diéguez et al. (2014) and Querol et al. (2016), who proposed a similar regionalization based on observations from air quality stations.

Figure 7a shows the absolute O_3 contribution of each tagged source at air quality stations by region along with the modelled and observed daily mean concentration during exceedances of 120 μgm^{-3} of the observed MDA8 ozone; Fig. 7b shows the respective fractional mean O_3 contribution. (Table S2 compiles de numerical values of Fig. 7.) We have excluded the ICON O_3 in Table S2 because its contribution is negligible after six days of spin-up. The spatial r between modelled and observed daily mean O_3 concentration during exceedances of the MDA8 target value is 0.79, which indicates that CALIOPE is able to reproduce reasonably well the spatial variability of O_3 during peak episodes in Spain.

The MED region represented by stations in the Balearic Islands shows the highest imported O_3 contribution (76%) because it is relatively far away from important anthropogenic NO_x+VOC sources in the IP. Under the ITL influence (July 25th and 31st), MED received air masses enriched with on-road traffic precursors from southern France and the NEIP, which enhanced O_3 production up to 7%. Shipping emissions in the Mediterranean contributed up to 8% of the O_3.

After MED, there is a cluster of regions along the Spanish Mediterranean coast (i.e., NEIP, EV and EIP) showing imported O_3 contributions between 60 and 68 % of the daily mean O_3 under exceedances. This is explained by their proximity to the eastern boundary and the frequent mesoscale phenomena enhancing the recirculation and accumulation of imported O_3 along the Spanish Mediterranean coasts. The contribution of road and non-road transport is similar (~11-16%) because these regions have both important roads and maritime trade routes. Note that the SIP region, which is also located in the Spanish Mediterranean coast, shows a daily mean imported O_3 concentration lower than the other Mediterranean regions (~57%) and the highest non-road transport contribution in Spain (19%). The main sink of imported O_3 are precursors resulting from dense shipping traffic through the Strait of Gibraltar, which have substantial impact in the O_3 production downwind (either in the Alboran Sea or the Gulf of Cadiz).

Atmospheric
Chemistry
and Physics
Discussions

The regions including the largest metropolitan areas in Spain are the CIP (Madrid) and the NEIP (Barcelona). Both regions show an imported O_3 contribution of ~60% and a similar contribution from the road transport sector (18 and 16%, respectively). However, the NEIP shows a slightly higher contribution from non-road transport (13 vs 10%) due to the influence of international shipping near coastal areas.

5

The northern and northwestern regions (NIP and NWIP) had relatively lower imported O_3 contributions (56-59%). The contribution of non-road transport was ~10-12%, slightly lower than in the Mediterranean coast, and that of road transport was also significant (~14-15%). The contribution from the industrial sector was one of the highest in the country (~5%) due to the influence of the large industrial facilities located in several areas of Galicia, Cantabria, Asturias, and the Basque

10   Country. The contribution from the energy sector in the NWIP region was the highest in Spain (~5%) due to emissions from large coal-fired power plants, including As Pontes, Meirama, Aboño, Guardo, and Compostilla.

The WIP had the lowest daily mean O_3 concentrations during days exceeding the O_3 Target Value (93.5 µgm^{-3}) and a high imported O_3 contribution (~63%). NO_x emissions in the WIP region are moderate (Fig. 4), which could explain the low daily

15   mean O_3 concentration. There is a significant contribution from traffic (14% for road transport and 11% for non-road transport) and industrial and energetic sectors (7%) to the daily mean O_3 concentrations. These anthropogenic contributions suggest that O_3 in the WIP is produced by precursors transported from the surrounding cities (Oporto, Lisbon and Madrid) and the highly industrialized areas in the NWIP and the NIP (Fig. 6).

20   The Guadalquivir Valley had the lowest imported O_3 contribution of the IP (~46%) and the highest daily O_3 concentration during days of exceedance. The relatively low imported O_3 contribution resulted from the titration effect driven by the high NO_x emissions from industrial and urban hotspots in the region. The on-road traffic was the highest anthropogenic contributor to O_3 (~18%) due to the emissions from three major cities (Sevilla, Huelva, and Cordoba). Although O_3 in Huelva may be overestimated (as discussed later), shipping is the second most important contributor to O_3 in the

25   Guadalquivir Valley (~17%) due to the important fluvial transport along the Guadalquivir River. (The Guadalquivir River is one of the most important routes for merchandise transport in Europe.) In fact, the non-road transport sector is the highest contributor (~17-19%) in Southern Spain, both in the Guadalquivir Valley and the SIP, also due to the dense maritime routes across the Strait of Gibraltar.

30   The following sections analyse the source apportionment results eight stations located in key regions (see Fig. 5). We analyse two regions with high on-road traffic contribution (CIP and NEIP), and two regions with high contribution from industry and energy production (NWIP and Guadalquivir Valley).

3.4.1 Central Iberian Peninsula

Figure 8 show the source apportionment time series of the hourly O_3 and NO_2 concentrations at two stations in the CIP, an urban station in Madrid (station 1 in Fig. 8a), and another one located in Guadalajara (station 2 in Fig. 8a), which is a medium size city affected by Madrid's urban plume. The model reproduces reasonably well the main processes and source
5   contributions, with a significant imported O_3 contribution in both stations.

In Madrid, the model reproduces the O_3 traffic cycle featuring the typical low O_3 concentrations (< 40 μgm^{-3}) in the early morning and in the afternoon due to O_3 titration (Fig. 8a). However, O_3 was overestimated (MB type D) during daytime peaks due to the overestimation of the NO_2 morning peaks during stagnant conditions. The NO_2 overestimation correlates
10   with the highest road transport contribution. The NO_2 overestimation in Madrid is inconsistent with the overall underestimation of NO_2 in urban areas due to the dilution effect. The results point towards a poor representation of the vertical mixing during the stagnant conditions. In urban areas downwind (Fig. 8b) the modelled O_3 shows a positive bias (MB type B) due to the underestimation of NO_2. While traffic NO_2 emissions in the largest urban areas (i.e. Madrid, Barcelona) are estimated at the road link level using specific data such as daily average traffic, mean speed circulation and
15   real-world vehicle fleet composition profiles, in medium size cities this information is not available and traffic emissions are estimated using emission factors that depend on population density (Guevara et al., 2013), which implies having a larger uncertainty in the results.

The O_3 contribution from the industrial sector (whose precursors could come from facilities in the southern MMA, Fig. 4)
20   reinforces the O_3 peaks up to ~10 μgm^{-3}, meanwhile the contribution from non-road transport increases systematically the background O_3 concentration by ~15 μgm^{-3}. The O_3 contribution from non-road transport in this region may arise from the Atlantic shipping route, Madrid's airports and the agricultural machinery operating in the surrounding rural areas.

Figure 8a and 8b also shows that the urban O_3 plume presents different intensity and distribution depending on the
25   meteorological pattern. Downwind of Madrid (Fig. 8b), stagnant conditions favour O_3 peaks exceeding 120 μgm^{-3} and on-road transport contributes up to 20-30 μgm^{-3} (e.g., July 25th). The highest O_3 concentrations (~160 μgm^{-3}) are modelled when westerly winds channelled along the Tajo valley carry the polluted air masses in a NE direction through the Tajo Valley, which results in a O_3 contribution of ~70 μgm^{-3} from road transport sector in areas downwind (see wind vectors in Fig. 8b on July 28th and 31st).

3.4.2 North-Eastern Iberian Peninsula

Figure 8c and 8d show the source apportionment time series at two stations in the NEIP, an urban station in Barcelona (station 3) and a remote rural area downwind (station 4). In the urban station, NO_2 levels of up to 100 μgm^{-3} affect O_3

Atmospheric
Chemistry
and Physics
Discussions

concentrations by titration during traffic peaks. In contrast, the rural station downwind depicts a higher O_3 and lower NO_2 concentration than the urban station.

Absolute O_3 biases in both stations are ~10 μgm^{-3} (MB type B). In the urban area, the modelled O_3 concentrations are in

5   agreement with the observations. The model suggests that O_3 mostly results from import and from the NO titration effect due to local road transport and industrial sources (Fig. 8c). However, the model presents some under/overestimation at nighttime, which could result from the NO_2 underestimation and complex mesoscale phenomena not captured by the model. Note that the O_3 diurnal cycle in the NEIP urban areas is less marked than in the CIP due to persistently high O_3 concentration at night (~60 μgm^{-3}). The breezes and mountain-valley winds contribute to the accumulation and recirculation of pollutants in this

10   region.

Despite of the slight overestimation of NO_2 concentration in rural areas, modelled O_3 peaks (> 120 μgm^{-3}) are highly correlated with observations (Fig. 8d), which suggests that overall the model reproduces the main transport paths, photochemical processes, and relative contributions from different sources. Imported O_3 is one of the main contributors to

15   ground-level O_3 (from 40 to 100 μgm^{-3}), but during peaks the on-road traffic contribution sharply increases up to 80 μgm^{-3}.

The O_3 concentration from the road transport sector arriving at rural areas in the NEIP, mainly comes from the Barcelona and surroundings as a result of the afternoon sea breezes (see wind vectors in Fig. 8c and 8d). However, under specific meteorological patterns these winds also carry precursors from other cities located in the NW Mediterranean Basin. For

20   example, on July 28th both the model and observations show that O_3 exceeded 120 μgm^{-3} in both urban and rural areas and the model attributed ~60% of it to regional anthropogenic sources (non-imported O_3). In the morning, two main meteorological phenomena favoured the transport of precursors towards the Western Mediterranean. First, the North African Thermal Low reinforced the sea breezes in the NEIP coast. Second, NW synoptic winds channelled between the Pyrenees and the French Central Massif towards the Golf of Lion transported precursors from urban areas upwind (e.g., Marseille,

25   Toulouse). In the afternoon, the sea breezes transported air masses enriched with O_3 and precursors inland. Other authors (Gangoiti et al., 2001) have hypothesized that high O_3 concentration in the Western Mediterranean Basin is influenced by transport from France via the Carcassonne gap. The present experiment cannot quantify the contribution of French cities to the O_3 concentration over the NEIP, but future studies could explicitly tag the emission from the French regions.

3.4.3 Guadalquivir Valley

30   The largest modelled O_3 overestimations are found in the Guadalquivir Valley (MB type D). Precursors emitted along the Guadalquivir Valley arise from large industrial facilities and a coastal power plant (Fig. S3), a few densely populated cities (notably Sevilla and Cordoba with more than 700,000 and 320,000 inhabitants, respectively), and the navigable river. The airflow in the region is controlled by the Atlantic synoptic conditions, the development of breezes in the coast of the Gulf of

Cadiz and the channelling through the Guadalquivir Valley (Adame et al., 2008). We have selected two stations along the Guadalquivir Valley to evaluate O_3, one in the urban area of Sevilla (station 5 in Fig. 9a), and one in a rural coastal area (station 6 in Fig. 9b). The contribution of anthropogenic sources to NO_2 at the coastal rural background station is low but still significant. The contribution of non-road transport is due the influence of one of the largest Spanish harbours. The

5   contribution of the energy sector to the O_3 concentration is also noticed (e.g., July 25th). As expected, the urban station (Fig. 9a) shows a high NO_2 concentration dominated by on-road traffic. NO_x from traffic is the main sink of O_3 in the city and the model reproduces the titration effect in agreement with observations (e.g., July 28th-31st).

High O_3 overestimations (10-30 μgm^{-3}) at both stations (Fig. 9a and b) were detected during July 25th-28th which

10   corresponds to intense and persistent SW winds transporting air masses from the Atlantic Sea along the Guadalquivir Valley, as shown by the wind vectors in Fig. 9a and b. Although the model overestimates O_3 concentrations, it reproduces the temporal variability. Our results suggest that the non-road transport sector is a significant contributor along the Guadalquivir Valley during these days. The impact of shipping emission on O_3 in the Guadalquivir Valley region is mainly evidenced by the relative high NO_x from ship exhaust (Fig. S3). NO_2 time series at the coastal station (Fig. 9b) indicates that the model

15   overestimates NO_2 concentrations in hours where the NO_2 contribution from non-road transport is the highest. The unrealistic NO_2 peaks from non-road transport suggest that shipping emissions are overestimated in the HERMESv2.0 model. HERMESv2.0 uses the EMEP gridded emission database at 50 km x 50 km horizontal resolution to estimate shipping emissions and spatially distributes them to the 4-km model domain using the marine routes reported by Wang et al. (2008). Marine traffic emissions estimated with current state-of-the-art methods, such as the use of data provided by Automatic

20   Identification System (AIS), show large discrepancies with the reported CEIP-EMEP gridded inventories both in term of totals and spatial distribution (Jalkanen et al., 2012), suggesting that uncertainties associated to current official emissions may be large. This factor, added to the 15% decrease of NO_x shipping emissions observed in Europe between 2009 (HERMESv2.0 base year) and 2012 (http://www.ceip.at) could explain the discrepancies observed.

25   O_3 peaks are highly biased (by ~40-50 μgm^{-3}) during stagnant conditions on July 28th-31st, especially in the urban station (station 5). During these days, measured NO_2 daily peaks increased up to 40 μgm^{-3}. Although the model reproduces the variability, it overestimates the concentration due to an excessive on-road transport contribution. As discussed for the CIP, under low dispersion conditions NO_2 concentrations are difficult to model due to complex mixing regimes.

3.4.4 Northwestern Iberian Peninsula

30   Figures 9c and 9d show the source apportionment time series at one urban (station 7) and one rural (station 8) background station in the NWIP. The urban station (Fig. 9c) located in Santiago de Compostela, a medium size city with ~100,000 inhabitants, shows a high NO_2 concentration with a dominant contribution from the road transport sector. Traffic NO_2 is the

main sink of urban O_3 via titration. Because NO_2 is underestimated, especially during stagnant conditions (July 24th-27th), O_3 concentrations are overestimated (MB category C).

In rural background areas (Fig. 9d), the modelled O_3 concentration is in general agreement with observations (MB category
5   B), but the model tends to underestimate the observed concentrations, particularly under weak winds. NO_2 is likely to be underestimated due to missing traffic emissions. As noted previously, traffic emissions are poorly constrained in small and medium size cities, due to a lack of detailed information. There is also additional uncertainty in the precursors emitted from the large coal power plants and industries in the region (Valverde et al., 2016b). Our study uses emissions for 2009, and it has been estimated that between 2009 and 2012 energy production in coal-fired power plants increased from 13.1% to 19.4%
10   (UNESA, 2012).

Despite the O_3 biases during stagnant conditions, the time series show that model reproduces reasonably well the observed O_3 variability under different synoptic conditions. O_3 reaches the highest concentration (~100/150 μgm^{-3} in urban/rural areas) under stagnant conditions (July 24th-27th) when the contribution of anthropogenic sources from all activity sectors is
15   the highest (60-70%). O_3 concentrations decrease down to ~70 μgm^{-3} under NW advective conditions (e.g., July 28th-30th) when the imported O_3 shows the highest contribution (80-90%). Saavedra et al. (2012) found that stationary anticyclones over the northern play an important role in the occurrence of high O_3 concentrations over the NWIP. Our results show that under these stagnant conditions O_3 concentrations are due largely to in situ production (photochemistry) from on-road traffic, shipping, power plants, and industry in almost the same proportion.

20

3.5 Imported ozone

These O_3 source apportionment results indicate that imported O_3 represents the highest contribution to ground-level O_3 concentration in southwestern Europe. Imported O_3 enters the IP4 domain through the boundaries; it includes the contribution of O_3 from the EU12 domain, which in turn includes the contribution of hemispheric O_3 from the MOZART-4
25   global model. The imported O_3 is as large as the background O_3 regionally produced within the IP. We note that the small biases at rural background stations obtained in the evaluation section indicate an overall high performance of the modelled background O_3 in the IP4 domain (Fig. S1). Given its importance, this section is devoted to analyse the importance of the imported O_3 in southwestern Europe. In particular, we aim to understand its high contribution within the IP, far from the model domain boundaries.

30

Figure 10 shows the vertical cross-sections at 6, 12, and 18 UTC for O_3 and NO_2 at a constant latitude (40.38° N) on July 25th, 28th and 30th. The model predicts a pronounced O_3 vertical gradient above a height of 4 km above sea level (asl), showing that O_3 in the free troposphere is, to a large extent, imported to the IP4 domain (Safieddine et al., 2014). As

Atmospheric
Chemistry
and Physics
Discussions

expected, NO_2 mixing ratios show a negative gradient with altitude as it is mainly emitted at the surface. In the morning, the sun starts to heat up the ground, producing convective thermals and forcing the growth of the mixing layer. At noon, the mixing height reaches its maximum, being the highest in the CIP (2-4 km) and decreasing towards the coast (< 1 km) (Fig. 10). At the mixing layer top the O_3-enriched air aloft is entrained into the mixing layer, mixing with O_3 and other pollutants

5   produced locally within the mixing layer. When the mixing height decreases, O_3 is left in the free troposphere forming high O_3 residual layers (Gangoiti et al., 2001) that contribute to the regional transport. Over the following days, these residual layers (composed of imported O_3 and local O_3 produced within the domain over previous days) can be entrained by fumigation into the mixing layer to reach the surface. This fumigation effect, previously described in the eastern USA (Zhang and Rao, 1999; Langford et al., 2015) and in the Western Mediterranean Basin (Kalabokas et al., 2017; Querol et al.,

10   2018), leads to a rapid increase in O_3 concentrations at ground level. The accumulation and recirculation of air masses is intensified along the Eastern Mediterranean coast (Millán et al., 1996, 2000; Gangoiti et al., 2001; Querol et al., 2017) by the action of the breezes and mountain-valley winds. Furthermore, the small deposition velocity of O_3 over the sea and its high atmospheric lifetime in the free troposphere contributes to enrich the O_3 background concentration (c.a. several weeks, Monks et al., 2015; Seinfeld and Pandis, 2016).

15

The O_3 fumigation effect was particularly intense on July 30th-31st, when a high O_3 levels are found in the free troposphere compared to previous days (Fig. 10). The analysis of the O_3 concentration map with the imported O_3 contributions (Fig. 6) indicates that ground-based O_3 is neither advected nor titrated; therefore, it can only result from vertical mixing. The high O_3 mixing ratio in the free troposphere was mainly due to O_3 advection entering the Atlantic boundary driven by westerlies (Fig.

20   3). We hypothesize that two events may have contributed to the increase of the O_3 concentration by long-range transport. First, a low-pressure system in the British Islands on July 28th could have transported significant O_3 amounts from the stratosphere to the free troposphere (Fig. S4). Second, O_3 episodes generated in mid-July over the Eastern USA predicted by the MOZART-4 model could have contributed to an increase in the O_3 transported from N America to Europe by the action of the prevailing westerlies (Fig. S4) associated with cyclonic systems along the ''warm conveyor belt'' (Pausata, et al.,

25   2012; Derwent et al., 2015).

4 Discussion and conclusions

We investigate the origin of ground-level O_3 concentration over southwestern Europe during the episode July 21st -31st, 2012. The period includes the two most frequent summer synoptic circulation patterns over the region: stagnant conditions with development of the Iberian Thermal Low (ITL) and North Western Advection (NWad). We used the Integrated Source

30   Apportionment Method (ISAM) within the CALIOPE system to estimate the main sources responsible of the high O_3 concentrations in receptor regions over the IP compared to the imported (regional and hemispheric) O_3 contribution. In addition, the source apportionment method has allowed an in-depth evaluation of the modelling system applied. Below, we

summarize the new findings from the source attribution study, we discuss the model uncertainties and we give a perspective on some of the regulatory implications, which may be applicable to other non-attainment regions.

4.1 Source apportionment results

The results demonstrate that the O_3 problem over the Western Mediterranean Basin is local, regional, and hemispheric. Long-range transport of O_3 from beyond the IP domain is the main contributor to the ground-level daily mean O_3 concentration (~45%) during peak episodes. The imported O_3 contribution ranges from 40% during O_3 peaks to 80% at night or during well-ventilated conditions. The absolute imported O_3 is higher in NEIP than in the central IP due to the recirculation and accumulation of pollutants along the Mediterranean. The high imported O_3 at the surface far away from the model boundaries is consistent with the high levels of O_3 in the free troposphere (resulting from local/regional layering and accumulation, and continental/hemispheric transport) along with intense vertical mixing during the day.

During high O_3 events, the imported O_3 is added to the local and regional anthropogenic contributions. The road transport is an important contributor to the O_3 concentration in rural areas downwind of the large cities in Spain. It contributed up to 16-18% of the daily mean O_3 concentration under exceedances of the target value for human health protection, and up to 70 μgm^{-3} on an hourly basis downwind of Barcelona and Madrid. The non-road transport sector is as significant as road transport inland (10-19% of the daily mean O_3 concentration during the peaks). There is a high influence of international shipping (13%), affecting the coastal areas in the Mediterranean and the southern IP (along the Strait of Gibraltar) with contributions of up to ~20 and ~30 $\mu g/m^3$, respectively. The energy and industrial sectors contribute ~6-11% of the daily mean O_3 concentration during the peaks and over all the receptor regions. As they usually are injected in high altitudes, their contribution extend way beyond their surroundings. The energy combustion sector (3%) and industrial and non-industrial combustion sectors (3%) have a mean contribution of 2-4 μgm^{-3}, going up to 4-6 μgm^{-3} in NO_x-limited areas (i.e., the western IP). The OTHR tag, which lumped the remaining sectors (i.e., SNAP 2, 5, 6, 9, and 11, see Table 1), is the fourth main contribution to the daily mean O_3 concentration during the days exceeding the target value (~2-8%). Future work should tag the biogenic sources as an individual sector as it is the main contributor to VOC emissions in Spain (i.e., ~70% in 2009 according to HERMESv2.0 model).

4.2 Model uncertainty

The modelled concentrations present uncertainties that are in the same range as the most recent inter-comparison studies using state-of-the-art air quality models. Our results show a good agreement between the modelled and observed O_3, which provides confidence in our source apportionment results.

In addition, our model evaluation together with the source apportionment results has allowed a better understanding of the origin of model errors. Under stagnant conditions, the model shows lower performances: in coastal areas, this may be related

to a poor representation of mesoscales processes such a sea breezes and recirculation; in Madrid, NO_2 overestimations may be due to a poor representation of the vertical mixing. There is likely an overestimation of shipping emissions, and an underestimation of road transport emissions in medium size cities.

5   Overall, the estimated imported O_3 depends on both the performance of the CALIOPE system over EU12, and on MOZART-4 at global scale. The evaluation of model in the EU12 domain using the European EIONET stations (not shown here) showed good skills for O_3 and its precursors. Furthermore, the source apportionment results have shown that O_3 local production could be as large as the imported O_3 , so the small biases at rural background stations indicate an overall high performance baseline background O_3 in the IP4 domain (Fig. S1). This study has not evaluated MOZART-4, but there are

10   many studies supporting its good performance. Several inter-comparison studies (e.g., EURODELTA and AQMEII) also found the importance of chemical boundary conditions to reproduce the O_3 background concentrations (Giordano et al. 2015; Bessagnet et al., 2016; Solazzo et al., 2017).

Our set-up involves some uncertainty in the estimation of the imported contribution of O_3. In reality, there is a fraction of the

15   imported O_3 that may have been generated within the IP4 domain before the period of simulation (including the spin-up). We have assumed that this fraction is negligible and future works should check to what extent this assumption is correct.

4.3 Regulatory implications

Our study has identified the main sources responsible of high O_3 in receptor regions in the Western Mediterranean Basin, but cannot predict whether emission abatement will have either a positive or negative effect in O_3 changes due to the non-

20   linearity of the O_3 generation process (Monks et al., 2015 and papers therein). Subsequent source sensitivity analysis tailoring the identified main contribution sources could predict how O_3 will respond to reductions in precursor emissions. Future source sensitivity studies are essential to define the most efficient abatement strategies to reduce high O_3 concentrations in the Western Mediterranean Basin. Complementarily, it would be important to know where the emission abatement strategies should be applied. To answer this question further source apportionment studies should be conducted

25   tagging both source activities and source regions.

This case study supports a relatively old conclusion by the European Commission (EC, 2004) pointing out that the effectiveness of abatement strategies for achieving compliance with the European air quality standards in southern Europe might be compromised by the long-range transport of O_3. This is especially true in Mediterranean regions (i.e., NEIP, EV

30   and EIP) where the contribution of imported O_3 is particularly dominant (60-68% of the daily mean O_3 concentration in episodes) as a result of the accumulation and recirculation of pollutants over the Mediterranean Basin. In those areas, if the long-range transport of O_3 is not reduced, the mean background level will not decrease making it more vulnerable to exceedances of the O_3 target values by enhanced local production under stagnant conditions.

Atmospheric
Chemistry
and Physics
Discussions

Reduction of the background O$_3$ concentration can be achieved by decreasing the concentrations of O$_3$ and precursors aloft. Given the polluted dome aloft the Western Mediterranean Basin during a typical O$_3$ episode, which may result from local/regional layering and accumulation, and continental/hemispheric transport, it will necessary and important to

5   implement emission reduction strategies on the hemispheric and continental scale. There is an urgent need of international collaboration at European and hemispheric level to reduce O$_3$ and its precursors. High background contribution to Iberian O$_3$ could represent a substantial future challenge to the attainment of O$_3$ limit values, which requires controlling hemispheric O$_3$ (EC, 2004; Fowler et al., 2013).

10   Besides the long-range transport contribution, O$_3$ peaks during episodes result from the local/regional photochemical formation from the transport and industrial sectors, and therefore regional emission reduction strategies are also urgent. The contribution from road transport determines O$_3$ peaks in rural areas (up to 70 µg/m^3) downwind of the main Spanish Metropolitan Areas (i.e., Madrid and Barcelona). To reduce O$_3$ peaks downwind of the Madrid city, a decrease of road transport emissions in the urban area would be effective. However, to reduce O$_3$ peaks downwind of the Barcelona city, the

15   reduction of road traffic emission in the city should be complemented with abatement strategies in other Mediterranean cities, especially in Southern France.

In the BMA the contribution from energy and industrial sectors to NO$_2$ concentration can be in the same range than the contribution from road transport (~40-60%, Fig. 8c). In contrast, in areas downwind of the BMA the contribution from

20   energy and industrial sectors to O$_3$ concentrations is relatively low compared with the contribution from road transport (Fig. 8d). The differences contribution to O3 concentration might link with the different reactivity of VOC for O$_3$ formation. Each VOC emission source emits a different mix of VOC, which makes a different contribution to photochemical ozone formation. For example, in the UK, Derwent et al. (2007) showed a higher photochemical O$_3$ creation potential for road transport emissions than for production processes and combustion. Future national policy actions to control the emissions of

25   VOC should tackle the sources that contribute more to photochemical O$_3$ formation.

Although the non-road transport contribution was found to be overestimated in coastal areas in the south of the IP in the present experiment, it cannot be neglected and actions controlling international shipping should be considered as important as those related with road transport especially in regions with big harbours (e.g., Huelva and Barcelona). Dalsøren et al.

30   (2010) indicated that annual O$_3$ concentration is increasing yearly in a range of 0.5-2.5 ppb in areas impacted by shipping activities. Recent studies indicate that shipping emissions are projected to increase significantly due to increases in transportation demand and traffic. As the Strait of Gibraltar is the only shipping route connecting the Atlantic Ocean with the Mediterranean Basin, the regulation of these emissions is key in order to control O$_3$ exceedances in Spain and the Mediterranean Basin. Shipping emissions can be regulated by each country within 400 km of coastlines, but policy-induced

controls for offshore emissions are very dependent on the success of adopted and proposed regulations within the International Maritime Organization.

5 In highly industrialized regions (i.e., Guadalquivir Basin and northwestern IP), abatement strategies affecting all sectors at regional scale could contribute to decrease the local formation of O_3 as the regional/local anthropogenic contribution can be greater than 50% during several days.

Overall, we find that the imported O_3 is the largest input to the ground-level O_3 concentration in the IP during episodes. In addition, during stagnant conditions, the emission from local anthropogenic activities in the IP control the O_3 peaks in areas 10 downwind of the main urban and industrial regions. Furthermore, ground-level O_3 concentrations are strongly affected by vertical downward mixing of O_3-rich layers in the free troposphere, which result from local/regional layering and accumulation, and continental/hemispheric transport. The importance of both imported and local contributions to the O_3 peaks in the IP demonstrates the need for detailed quantification of both contributions to high O_3 concentrations for local O_3 management. Furthermore, the influence of local sources and topographical and meteorological conditions in the high O_3 15 concentration indicate the importance of designing O_3 abatement policies at local scale.

This work has identified local and imported contributions to O_3 concentration during an episode in a particular area in southwestern Europe. However, further detailed and longer O_3 source apportionment studies targeting other nonattainment regions in Europe are necessary prior to define local mitigation measurements that complement national and European-wide 20 strategies to reach the European O_3 objectives.

Data availability

Air quality measurements are available at the EIONET database (https://www.eea.europa.eu/data-and-maps/data/airbase-the-european-air-quality-database-7). The CMAQ code is available at the https://www.cmascenter.org/. The WRF-ARW code is 25 available at http://www2.mmm.ucar.edu/wrf/users/download/get_source.html. Download Mozart-4 outputs are available at http://www.acd.ucar.edu/wrf-chem/mozart.shtml. The program that generates CMAQ boundary conditions from MOZART-4 output is available at: http://www.camx.com/getmedia/a0c2d710-6187-47bb-af3f-bd9b4a4d19bb/mozart2camx-12jul17.tgz. The HERMESv2 outputs are available upon request. The modelled data in this study are available upon request from the corresponding author.

30

Appendix A
Table 1A shows the acronyms used in the text.

BCON	Chemical boundary conditions to IP4, also named as imported O_3 contribution
BMA	Barcelona Metropolitan Area
CIP	Central Iberian Peninsula
CMAQ	Community Multiscale Air Quality model
EIP	Eastern Iberian Peninsula
EU12	European domain at 12-km horizontal resolution
EV	Ebro Valley
GV	Guadalquivir Valley
IP	Iberian Peninsula
IP4	Iberian Peninsula domain at 4-km horizontal resolution
ISAM	Integrated Source Apportionment Method
MDA8	Maximum daily 8-hour average concentration
MMA	Madrid Metropolitan Area
MED	Mediterranean Sea
NEIP	Northeastern Iberian Peninsula
NIP	Northern Iberian Peninsula
NWIP	Northwestern Iberian Peninsula
SIP	Southern Iberian Peninsula
SNAP1	Emission sector on combustion in energy
SNAP34	Emission sector on combustion and processes in industry
SNAP7	Emission sector on road transport, exhaust and non-exhaust
SNAP8	Emission sector on non-road transport (international shipping)
WIP	Western Iberian Peninsula
WRF	Weather Research and Forecasting Model

Appendix B

Definition of the discrete statistics used in the evaluation: correlation coefficient (Eq. B1), mean bias (Eq. B1) and root mean squared error (Eq. B3). Where $C_m(x, t)$ and $C_o(x,t)$ are the modelled and observed concentrations at a location (x) and time (t); N is the number of pairs of data. $\overline{C_m}$ and $\overline{C_o}$ are the modelled and observed mean concentrations over the whole period, respectively.

$$r = \frac{\sum_{i=1}^{N}(C_m(x,t) - \bar{C}_m)(C_o(x,t) - \bar{C}_o)}{\sqrt{\sum_{i=1}^{N}(C_m(x,t) - \bar{C}_m)^2}\sqrt{\sum_{i=1}^{N}(C_o(x,t) - \bar{C}_o)^2}} \tag{B1}$$

$$MB = \frac{1}{N}\sum_{i=1}^{N}\left(C_m(x,t) - C_0(x,t)\right) \tag{B2}$$

Atmospheric
Chemistry
and Physics
Discussions

$$RMSE = \sqrt{\frac{1}{N}\sum_{i=1}^{N}(C_m(x,t) - C_o(x,t))^2}$$ (B3)

Acknowledgments

References

Adame, J.A., Lozano, A., Bolívar, J.P., De la Morena, B.A., Contreras, J., amd Godoy, F.: Behaviour, distribution and variability of surface ozone at an arid region in the south of Iberian Peninsula (Seville, Spain), Chemosphere, 70, 841-849, doi: 10.1016/j.chemosphere.2007.07.009, 2008.

Aksoyoglu, S., Baltensperger, U., and Prévôt, A. S. H.: Contribution of ship emissions to the concentration and deposition of air pollutants in Europe, Atmos. Chem. Phys., 16, 1895–1906, doi:10.5194/acp-16-1895-2016, 2016.

Appel, K. W., Pouliot, G. A., Simon, H., Sarwar, G., Pye, H. O. T., Napelenok, S. L., Akhtar, F., and Roselle, S. J.: Evaluation of dust and trace metal estimates from the Community Multiscale Air Quality (CMAQ) model version 5.0, Geosci. Model Dev., 6, 883–899, doi:10.5194/gmd-6-883-2013, 2013.

Baldasano, J.M., Jiménez-Guerrero, P., Jorba, O., Pérez, C., López, E., Güereca, P., Martín, F., Vivanco, M.G., Palomino, I., Querol, X., Pandolfi, M., Sanz, M.J., Diéguez, J.J.: Caliope: an operational air quality forecasting system for the Iberian Peninsula, Balearic islands and Canary islands e first annual evaluation and ongoing developments. Adv. Sci. Res. 2, 89-98, 2008.

Baldasano, J.M., Pay, M.T., Jorba, O., Gassó, S., and Jiménez-Guerrero, P.: An annual assessment of air quality with the CALIOPE modeling system over Spain. Sci Total Environ, 409, 2163-2178, doi: 10.1016/j.scitotenv.2011.01.041, 2011.

Basart, S., Pérez, C., Nickovic, S., Cuevas, E., and Baldasano, J.M.: Development and evaluation of the BSC-DREAM8b dust regional model over Northern Africa, the Mediterranean and the Middle East, Tellus B 64, 18539, doi: 10.3402/tellusb.v64i0.18539, 2012.

Bessagnet, B., Pirovano, G., Mircea, M., Cuvelier, C., Aulinger, A., Calori, G., Ciarelli, G., Manders, A., Stern, R., Tsyro, S., Gar- cía Vivanco, M., Thunis, P., Pay, M.-T., Colette, A., Couvidat, F., Meleux, F., Rouïl, L., Ung, A., Aksoyoglu, S.,

Baldasano, J. M., Bieser, J., Briganti, G., Cappelletti, A., D'Isidoro, M., Fi- nardi, S., Kranenburg, R., Silibello, C., Carnevale, C., Aas, W., Dupont, J.-C., Fagerli, H., Gonzalez, L., Menut, L., Prévôt, A. S. H., Roberts, P., and White, L.: Presentation of the EURODELTA III intercomparison exercise – evaluation of the chemistry transport models' performance on criteria pollutants and joint analysis with meteorology, Atmos. Chem. Phys., 16, 12667–12701, doi:10.5194/acp-16-12667-2016, 2016.

Booker, F. L., Muntifering, R., McGrath, M., Burkey, K., Decoteau, D., Fiscus, E., Manning, W., Krupa, S., Chappelka, A. and Grantz, D.: The ozone component of global change: potential effects on agricultural and horticultural plant yield, product quality and interactions with invasive species, J. Integrative Plant Biol., 51, 337-351, doi: 10.1111/j.1744-7909.2008.00805.x, 2009.

Borrego, C., Monteiro, A., Martins, H., Ferreira, J., Fernandes, A.P., Rafael, S., Miranda, A.I., Guevara, M., and Baldasano, J.M.: Air quality plan for ozone: an urgent need for North Portugal, Air Qual. Atmos. Health 8, 352–366, doi: 10.1007/s11869-015-0352-5, 2015.

Butler, T., Lupascu, A., Coates, J., and Zhu, S.: TOAST 1.0: Tropospheric Ozone Attribution of Sources with Tagging for CESM 1.2.2, Geosci. Model Dev. Discuss., https://doi.org/10.5194/gmd-2018-59, in review, 2018.

Byun, D.W., and Schere, K.L.: Review of the governing equations, computational algorithms and other components of the Models-3 Community Multiscale Air Quality (CMAQ) Modeling System, Appl. Mech. Rev., 59, 51–77, doi: 10.1115/1.2128636, 2006.

Carslaw, D. C., and Ropkins, K.: Openair—an R package for air quality data analysis. Environ. Modell. Softw., 27, 52-61, doi: 10.1016/j.envsoft.2011.09.008, 2012.

Carter, W.P.L.: Development of ozone reactivity scales for volatile organic compounds, J. Air Waste Manage. Assoc., 45, 4438-4445, doi: 10.1080/1073161X.1994.10467290, 1994.

Crutzen, P., J.: Photochemical reactions initiated by an influencing ozone in the unpolluted troposphere. Tellus, 26, 47-57, doi: 10.1111/j.2153-3490.1974.tb01951.x, 1975.

Dalsøren, S. B., Eide, M. S., Myhre, G., Endresen, O., Isaksen, I. S. A., and Fuglestvedt, J. S.: Impacts of the large increase in international ship traffic 2000–2007 on tropospheric ozone and methane, Environ. Sci. Technol., 44, 2482–2489, doi: 10.1021/es902628e, 2010.

Demuzere, M., Trigo, R. M., Vila-Guerau de Arellano, J. and van Lipzig, N. P. M.: The impact of weather and atmospheric circulation on O_3 and PM10 levels at a rural mid-latitude site, Atmos. Chem. Phys. 9, 2695-2714, doi: 10.5194/acp-9-2695-2009, 2009.

Derwent, R., Jenkin, M.E., Passant, N.R., and Pilling, M.J.: Photochemical ozone creation potentials (POCPs) for different emission sources of organic compounds under European conditions estimated with a Master Chemical Mechanism, Atmos. Environ., 41, 2570-2579, doi:10.1016/j.atmosenv.2006.11.019, 2007.

Derwent, R., Utembe, S.R., Jenkin, M.E., and Shallcross, D.E.: Tropospheric ozone production regions and the intercontinental origins of surface ozone over Europe. Atmos. Environ., 112, 216-224, doi: 10.1016/j.atmosenv.2015.04.049, 2015.

Diéguez, J.J., Calatayud, V., and Mantilla, E.: Informe final. Memoria Técnica Proyecto CONOZE (Contaminación por Ozono en España). 139 pp. [Available at: http://www.mapama.gob.es/es/calidad-y-evaluacion-ambiental/temas/atmosfera-y-calidad-del-aire/Informe_t%C3%A9cnico_CONOZE[1]_tcm7-330956.pdf, last access 7 September 2017], 2014.

Domínguez-López, D., Adame, J.A., Hernández-Ceballos, M.A., Vaca, F., De la Morena, B.A., and Bolívar, J.P.: Envrion. Monit. Assess., 186, 5337-5351, 2014.

EC: European Commission Decision of 19 March 2004. Concerning guidance for implementation of Directive 2002/3/EC of the European Parliament and the Council relating to ozone in ambient air (2004/279/EC). Official Journal of the European Union L87/50 of 25.3.2004., 2004.

Eder, B., Kang, D., Mathur, R., Yu, S., and Schere, K.: An operational evaluation of the Eta-CMAQ air quality forecast model, Atmos. Environ., 40, 4894-4905, doi: 10.1016/j.atmosenv.2005.12.062, 2006.

EEA: Air pollution by ozone across Europe during summer 2012, EEA Report No 3/2013.. 48 pp. doi: http://dx.doi.org/10.2800/70933, 2013.

EEA: Air quality in Europe – 2017 report. EEA Report, No 13/2017. ISSN 978-92-9213-920-9, 2017.

EMEP-CCC: Air pollution trends in the EMEP region between 1990 and 2012, EMEPCCC-Report 2016/1 (102 pp., http://icpvegetation.ceh.ac.uk/publications/documents/EMEP_Trends_Report_final_published.pdf), 2016.

Emmons, L. K., Walters, S., Hess, P. G., Lamarque, J. F., Pfister, G. G., Fillmore, D., and Orlando, J.: Description and evaluation of the Model for Ozone and Related chemical Tracers, version 4 (MOZART-4). Geosci. Model Dev., 3(1), 43-67, doi: 10.5194/gmd-3-43-2010, 2010.

Escudero, M., Lozano, A., Hierro, J., del Valle, J., and Mantilla, E.: Urban influence on increasing ozone concentrations in a characteristic Mediterranean agglomeration, Atmos. Environ., 99, 322-332, doi: 10.1016/j.atmosenv.2014.09.061, 2014.

Ferreira, J., Guevara, M., Baldasano. J.M., Tchepel, O., Schaap, M., Miranda, A.I., and Borrego, C.: A comparative analysis of two highly spatially resolved atmospheric emission inventories that are available in Europe, Atmos. Environ., 75, 43-57, doi:10.1016/j.atmosenv.2013.03.052., 2013.

Foley, K. M., Roselle, S. J., Appel, K. W., Bhave, P. V., Pleim, J. E., Otte, T. L., and Nolte, C. G.: Incremental testing of the Community Multiscale Air Quality (CMAQ) modeling system version 4.7, Geosci. Model Dev., 3(1), 205-226, doi:10.5194/gmd-3-205-2010, 2010.

Fowler, D., Brunkreef, B., Fuzzi, S., Monks, P.S., Sutton, M.A., Brasseur, G.P., Friedrich, R., Passante, L.G., and Jimenez-Mingo, J.M.: Research Findings in support of the EU Air Quality Review. Publications office of the European Union, Luxembourg, 2013.

Gangoiti, G., Millán, M.M., Salvador, R., and Mantilla, E.: Long-range transport and re-circulation of pollutants in the western Mediterranean during the project Regional Cycles of Air Pollution in the West-Central Mediterranean Area, Atmos. Environ. 35, 6267–6276, doi:10.1016/S1352-2310(01)00440-X, 2001.

Gangoiti G., Alonso L., Navazo M., Albizuri A., Pérez-Landa G., Matabuena M., Valdenebro V., Maruri M., García J.A., and Millán M. M.: Regional transport of pollutants over de Bay of Biscay: analysis of an ozone episode under a blocking anticyclone in west-central Europe, Atmos. Environ., 36, 1349-1361, doi: 10.1016/S1352-2310(01)00536-2, 2002.

Gangoiti G., Albizuri A., Alonso L., Navazo M., Matabuena M., Valdenebro V., García J.A., and Millán M. M.: Sub-continental transport mechanisms and pathways during two ozone episodes in northern Spain, Atmos. Chem. Phys., 6, 1469-1484, doi: 10.5194/acp-6-1469-2006, 2006.

Gerasopoulos, E., Kouvarakis, G., Vrekoussis, M., Kanakidou, M., and Mihalopoulos, N.: Ozone variability in the marine boundary layer of the Eastern Mediterranean based on 7-year observations, J. Geophys. Res., 110, D15309, doi:10.1029/2005JD005991, 2005.

Giordano, L., Brunner, D., Flemming, J., et al.: Assessment of the MACC reanalysis and its influence as chemical boundary conditions for regional air quality modeling in AQMEII-2. Atmos. Envrion., 115, 371-388, doi: 10.1016/j.atmosenv.2015.02.034, 2015.

Gonçalves, M., Jiménez-Guerrero, P., and Baldasano, J.M.: Contribution of atmospheric processes affecting the dynamics of air pollution in South-Western Europe during a typical summertime photochemical episode, Atmos. Chem. Phys. 9, 849–864, doi: 10.5194/acp-9-849-2009, 2009.

Guenther, A., Karl, T., Harley, P., Wiedinmyer, C., Palmer, P., and Geron, C.: Estimates of global terrestrial isoprene emissions using MEGAN (Model of Emissions of Gases and Aerosols from Nature), Atmos. Chem. Phys. 6, 3181–3210, doi: 10.5194/acp-6-3181-2006, 2006.

Guevara, M., Martínez, F., Arévalo, G., Gassó, S., and Baldasano, J.M.: An improved system for modelling Spanish emissions: HERMESv2.0, Atmos. Environ., 81, 209–221, doi: 10.1016/j.atmosenv.2013.08.053, 2013.

Guevara, M., Pay, M.T., Martínez, F., Soret, A., van der Gon, H.D., and Baldasano, J.M.: Inter-comparison between HERMESv2.0 and TNO-MACC-II emission data using the CALIOPE air quality system (Spain), Atmos. Environ. 98, 134–145, doi: 10.1016/j.atmosenv.2014.08.067, 2014.

Holloway, T., Fiore, A., and Galanter Hastings, M.: Intercontinental transport of air pollution: will emerging science lead to a new hemispheric treaty?, Environ. Sci. Technol. 37, 4535–42, doi: 10.1021/es034031g, 2003.

Im, U., Bianconi, R., Solazzo, E., et al.: Evaluation of operational on-line-coupled regional air quality models over Europe and North America in the context of AQMEII phase 2. Part I: Ozone. Atmos. Enrion., 115, 404-420, doi: 10.1016/j.atmosenv.2014.09.042, 2015.

Jacob, D., and Winner, D.: Effect of climate change on air quality, Atmos. Environ., 43, 51–63, doi: 10.1016/j.atmosenv.2008.09.051, 2009.

Jalkanen, J.-P., Johansson, L., Kukkonen, J., Brink, A., Kalli, J., and Stipa, T.: Extension of an assessment model of ship traffic exhaust emissions for particulate matter and carbon monoxide, Atmos. Chem. Phys., 12, 2641-2659, doi: 10.5194/acp-12-2641-2012, 2012.

Jiménez, P., Lelieveld, J., Baldasano, J.M.: Multiscale modelling of air pollutants dynamics in the northwestern Mediterranean basing during a typical summertime episode. J. Geophys. Res., 111, D18306, doi: 10.1029/2005JD006516, 2006.

Jorba, O., Pérez, C., Rocadenbosch, F., Baldasano, J.M.; Cluster analysis of 4-Day Back Trajectories Arriving in the Barcelona Area, Spain, from 1997 to 2002. J. Appl. Meteorol, 43, 887-901, 2004.

Kalabokas, P., Hjorth, J., Foret, G., Dufour, G., Eremenko, M., Siour, G., Cuesta, J., and Beekmann, M.: An investigation on the origin of regional springtime ozone episodes in the western Mediterranean, Atmos. Chem. Phys., 17, 3905–3928, https://doi.org/10.5194/acp-17-3905-2017, 2017.

Karamchandani, P., Long, Y., Pirovano, G., Balzarini, A., and Yarwood, G.: Source-sector contributions to European ozone and fine PM in 2010 using AQMEII modeling data. Atmos. Chem., Phys., 17, 5643-5664, doi: 10.5194/acp-17-5643-2017, 2017.

Kranenburg, R., Segers, A.J., Hendriks, C., and Schaap, M.: Source apportionment using LOTOS-EUROS: module description and evaluation, Geosci. Model Dev., 6, 721-733, doi: 10.5194/gmd-6-721-2013, 2013.

Kwok, R. H. F., Napelenok, S. L., and Baker, K. R.: Implementation and evaluation of PM 2.5 source contribution analysis in a photochemical model. Atmos. Environ., 80, 398-407, doi: 10.1016/j.atmosenv.2013.08.017, 2013.

Kwok, R.H.F., Baker, K.R., Napelenok, S.L., and Tonnesen, G.S.: Photochemical grid model implementation and application of VOC, NO_x, and O_3 source apportionment. Geosci. Model Dev. 8, 99–114, doi: 10.5194/gmd-8-99-2015, 2015.

Lateb, M., Meroney, R.N., Yataghene, M., Fellouah, H., Saleh, F., and Boufadel, M.C.: On the use of numerical modelling for near-field pollutant dispersion in urban environments – A review, Environ. Poll., 208, 271-283, doi: 10.1016/j.envpol.2015.07.039, 2016.

Langford, A. O., Sen, C. J., Alvarez, R. J., Brioude, J., Cooper, O. R., Holloway, J. S., Lind, M. Y., Marchbanksa, R. D., Pierce, R. B., Sandberg, S. P., Weickmann, A. M., and Williams, E. J.: An Overview of the 2013 Las Vegas Ozone Study (LVOS): Impact of stratospheric intrusions and long-range transport on surface air quality, Atmos. Environ., 109, 305–322, 2015.

Lelieveld, J., Berresheim, H., Borrmann, S., Crutzen, P. J., Dentener, F. J., Fischer, H., Feichter, J., Flatau, P. J., Heland,J., Holzinger, R., Korrmann, R., Lawrence, M. G., Levin, Z.,Markowicz, K.M., Mihalopoulos, N., Minikin, A., Ramanathan,V., de Reus, M., Roelofs, G. J., Scheeren, H. A., Sciare, J., Schlager, H., Schultz, M., Siegmund, P., Steil, B., Stephanou, E. G., Stier, P.,Traub, M.,Warneke, C.,Williams, J.,and Ziereis, H.: Global air pollution crossroads over the Mediterranean, Science, 298, 794–799, 2002.

Millán, M.M.: Regional processes and long range transport of air pollutants in Southern Europe. The experimental evidence. In: Angeletti, G. (Ed.), Physico-chemical Behaviour of Atmospheric Pollutants: Proceedings of the Sixth European Symposium. European Commission, Luxembourg, pp. 445–459, 1994.

Millán, M.M., Salvador, R., Mantilla, E., and Artiñano, B.: Meterology and photochemical air pollution in southern Europe: experimental results from EC research projects. Atmos. Environ., 30, 1909-1924, doi: 10.1016/1352-2310(95)00220-0, 1996.

Millán, M.M., Salvador, R., Mantilla, E., and Kallos, G.: Photooxidant dynamics in the Mediterranean basin in summer: results from European research projects, J. Geophys. Res., 102, 8811–8823, doi: 10.1029/96JD03610, 1997.

Millán, M.M., Mantilla, E., Salvador, R., Carratalá, A., Sanz, M.J., Alonso, L., Gangoiti, G., and Navazo, M.: Ozone cycles in the western Mediterranean basin: interpretation of monitoring data in complex coastal terrain, J. Appl. Meteorol. 39, 487–508, doi: 10.1175/1520-0450(2000)039<0487:OCITWM>2.0.CO;2, 2000.

Millán, M.M.: Extreme hydrometeorological events and climate change predictions in Europe, J. Hydrol., 518, 206-224, doi: 10.1016/j.jhydrol.2013.12.041,2014.

Monks, P. S., Archibald, A.T., Colette, A., Cooper, O., Coyle, M., Derwent, R., Fowler, D., Granier, C., Law, K.S., Mills, G.E., Stevenson, D.S., Tarasova, O., Thouret, V., von Schneidemesser, E., Sommariva, R., Wild, O., and Williams, M.L.: Tropospheric ozone and its precursors from the urban to the global scale from air quality to short-lived climate forcer, Atmos. Chem. Phys. 15, 8889–8973, doi: 10.5194/acp-15-8889-2015, 2015

Otero, N., Sillmann, J., Schnell, J.L., Rust, H.W., and Butler, T.: Synoptic and meteorological drivers of extreme ozone concentration over Europe. Environ., Res. Lett., 11, 024005, doi: 10.1088/1748-9326/11/2/024005, 2016.

Orru, H., Andersson, C., Ebi, K. L., Langner, J., Åström, C.,and Forsberg, B.: Impact of climate change on ozone-related mortality and morbidity in Europe, Eur, Respir. J., 41(2), 285-294, doi: 10.1183/09031936.00210411, 2013.

Pausata, F.S.R, Pozzoli, L., Vignati, E., and Dentener, F.J.: North Atlantic Oscillation and tropospheric ozone variability in Europe: model analysis and measurements intercomposarisons, Atmos. Chem. Phys., 12, 6357-6376, doi: 10.5194/acp-12-6357-2012, 2012.

Pay, M.T., Martínez, F., Guevara, M., and Baldasano, J.M.: Air quality at kilometre scale grid over Spanish complex terrains. Geosci. Model Dev. 7, 1979–1999, doi: 10.5194/gmd-7-1979-2014, 2014.

Pérez, C., Sicard, M., Jorba, O., Comerón, A., and Baldasano, J. M.: Summertime re-circulations of air pollutants over the north-eastern Iberian coast observed from systematic EARLINET lidar measurements in Barcelona. Atmos. Environ., 38, 3983-4000, doi: 10.1016/j.atmosenv.2004.04.010, 2004.

Querol, X., Alastuey, A., Reche, C., Orio, A., Pallares, M., Reina, F., Dieguez, J.J., Mantilla, E., Mantilla, M., Alonso, L, Gangoiti, G., and Millán, M.: On the origin of the highest ozone episodes in Spain, Sci. Tot. Environ., 572, 379-389, doi: 10.1016/j.scitotenv.2016.07.193, 2016.

Querol, X., Gangoiti, G., Mantilla, E., Alastuey, A., Minguillón, M.C., Amato, F., Reche, C., Viana, M., Moreno, T., karanasiou, A., Rivas, I., Pérez, N., Ripoll, A., Brines, M., Ealo, M., Pandolfi, M., Lee, H.-K., Eun, H.-R., Park, Y.-H.,

Escudero, M., Beddows, D., Harrison, R.H., Bertrand, A., Marchand, N., Lyasota, A., Codina, B., Olid, M., Udina, M., Jiménez-Esteve, B., Soler, R.M., Alonso, L., Millán-M., and Ahn, K.-Ho.: Phenomenology of high ozone episodes in NE Spain, Atmos. Chem. Phys., 17, 2817-2838, doi: 10.5194/acp-17-2817-2017, 2017.

Querol, X., Alastuey, A., Gangoiti, G., Perez, N., Lee, H. K., Eun, H. R., Park, Y., Mantilla, E., Escudero, M., Titos, G., Alonso, L., Temime-Roussel, B., Marchand, N., Moreta, J. R., Revuelta, M. A., Salvador, P., Artíñano, B., García dos Santos, S., Anguas, M., Notario, A., Saiz-Lopez, A., Harrison, R. M., Millán, M., and Ahn, K.-H.: Phenomenology of summer ozone episodes over the Madrid Metropolitan Area, central Spain, Atmos. Chem. Phys., 18, 6511-6533, https://doi.org/10.5194/acp-18-6511-2018, 2018.

R Core Team: R: A language and environment for statistical computing. R Foundation for Statistical Computing, Vienna, Austria. Available at: http://www.R-project.org/, 2015.

Reis, S., Simpson, D., Friedrich, R., Jonson, J. E., Unger, S., and Obermeier, A.: Road traffic emissions – predictions of future contributions to regional ozone levels in Europe, Atmos. Environ., 34, 4701–4710, doi: 10.1016/S1352-2310(00)00202-8, 2000.

Reff, A., Bhave, P. V., Simon, H., Pace, T. G., Pouliot, G. A., Mobley, J. D., and Houyoux, M.: Emissions inventory of PM2.5 trace elements across the United States, Environ. Sci. Technol., 43, 5790–5796, doi:10.1021/es802930x, 2009.

Richards, N. A. D., Arnold, S. R., Chipperfield, M. P., Miles, G., Rap, A., Siddans, R., Monks, S. A., and Hollaway, M. J.: The Mediterranean summertime ozone maximum: global emission sensitivities and radiative impacts, Atmos. Chem. Phys., 13, 2331–2345, doi:10.5194/acp-13-2331-2013, 2013.

Saavedra, S., Rodríguez, A., Taboada, J. J., Souto, J. A., and Casares, J. J.: Synoptic patterns and air mass transport during ozone episodes in northwestern Iberia. Sci. Tot. Environ., 441, 97-110, doi: 10.1016/j.scitotenv.2012.09.014, 2012.

Safieddine, S., Boynard, A., Coheur, P.-F., Hurtmans, D., Pfister, G., Quennehen, B., Thomas, J. L., Raut, J.-C., Law, K. S., Klimont, Z., Hadji-Lazaro, J., George, M., and Clerbaux, C.: Summertime tropospheric ozone assessment over the Mediterranean region using the thermal infrared IASI/MetOp sounder and the WRF-Chem model, Atmos. Chem. Phys., 14, 10119-10131, doi:10.5194/acp-14-10119-2014, 2014.

Saiz-Lopez, A., Borge, R., Notario, A., Adame, J.A., de la Paz, D., Querol, X., Artíñano, B., Gómez-Moreno, F.J., and Cuevas, C.A.: Unexpected increase in the oxidation capacity of the urban atmosphere of Madrid, Spain, Sci. Rep., 7, 45956, doi: 10.1038/srep45956, 2017.

Sarwar, G., Simon, H., Bhave, P., and Yarwood, G.: Examining the impact of heterogeneous nitryl chloride production on air quality across the United States, Atmos. Chem. Phys., 12, 6455–6473, doi:10.5194/acp-12-6455-2012, 2012.

Sartelet, K. N., Couvidat, F., Seigneur, C., and Roustan, Y., 2012. Impact of biogenic emissions on air quality over Europe and North America, Atmos. Environ., 53, 131–141, doi: 10.1016/j.atmosenv.2011.10.046, 2012.

Seinfeld, J. H., Pandis, S. N.: Atmospheric chemistry and physics: from air pollution to climate change. John Wiley & Sons, 2016.

Sharma, S., Sharma, P., and Khare, M.: Photo-chemical transport modelling of tropospheric ozone: a review, Atmos. Environ., 159, 34-54, doi: 10.1016/j.atmosenv.2017.03.047, 2017.

Sicard, P., Serra, R., and Rossello, P.: Spatiotemporal trends in ground-level ozone concentrations and metrics in France over the time period 1999-2012, Environ. Res., 149, 122-144, doi: 10.1016/j.envres.2016.05.014, 2016.

5 Skamarock, W.C., and Klemp, J.B.: A time-split nonhydrostatic atmospheric model for weather research and forecasting applications, J. Comput. Phys. 227, 3465–3485, doi: 10.1016/j.jcp.2007.01.037, 2008.

TRANSPHORM: Source Contributions of Transport Emissions for European Air Quality and Exposure, Deliverable 2.4.4,   available   at: http://www.transphorm.eu/Portals/51/Documents/Deliverables/New%20Deliverables/D2.4.4%20Source%20contributions%2

10 0of%20transport%20emissions%20for%20European%20air%20quality%20and%20exposure.pdf   (last access: 11 August 2017), 2014.

Solberg, S., Hov, Ø., Søvde, A., Isaksen, I.S.A., Coddeville, P., De Backer, H., Foster, C., Orsolini, Y., and Uhse, K.: European surface ozone in the extreme summer 2003. J. Geophys. Res., 113, D07307, doi:10.1029/2007JD009098, 2008.

UNECE: Hemispheric transport of air pollution 2010. Part A: ozone and particulate matter. Air Pollution Studies, 17.

15 UNECE, LRTAP, Task Force on Hemispheric Transport of Pollutants HTAP 2010: Part A. Ozone and Particulate Matter (278 pp, ECE/EB.AIR/100, ISBN 978–92–1-117043-6,), 2010.

UNESA: Spanish Electricity Industry Association. Electricity Statistical Report 2012. Available at: http://www.unesa.es/biblioteca/category/10-memorias, 2012.

Valdenebro, V., Gangoiti, G., Albizuri, A., Alonso, L., Navazo, M., García, J.A., Iza, J., and Millán, M.M.: Buil-up and

20 decay of two ozone episodes through northern Iberia and southern France – An inter-regional transport analysis, Atmos. Environ., 45, 1591-1603, doi: 10.1016/j.atmosenv.2010.12.031, 2011.

Valverde, V., Pay, M.T., and Baldasano, J.M.: Circulation-type classification derived on a climatic basis to study air quality dynamics over the Iberian Peninsula, Int. J. Climatol. 35 (8), doi: 10.1002/joc.4179, 2014.

Valverde, V., Pay, M.T., and Baldasano, J.M.: Ozone attributed to Madrid and Barcelona on-road transport emissions:

25 characterization of plume dynamics over the Iberian Peninsula, Sci. Total Environ. 543, 670–682, doi: 10.1016/j.scitotenv.2015.11.070, 2016a.

Valverde, V., Pay, M.T., and Baldasano, J.M.: A model-based analysis of SO and NO dynamics from coal-fired power plants under representative synoptic circulation types over the Iberian Peninsula, Sci. Total Environ., 541, 701-713, doi: 10.1016/j.scitotenv.2015.09.111, 2016b.

30 Wagstrom, K.M., Pandis, S.N., Yarwood, G., Wilson, G.M., and Morris, R.E.: Development and application of a computationally efficient particulate matter apportionment algorithm in a three dimensional chemical transport model, Atmos. Environ., 42, 5650-5659, doi: 10.1016/j.atmosenv.2008.03.012, 2008.

Wang, C., Corbett, J.J., Firestone, J.: Improving Spatial Representation of Global Ship Emissions Inventories, Environ. Sci. Technol., 42, 193-199, doi: 10.1021/es0700799, 2008.

Atmospheric
Chemistry
and Physics
Discussions

WHO: Review of evidence on health aspects of air pollution - REVIHAAP project: technical report. WHO Regional Office for Europe, Copenhagen (302 pp., http://www.euro.who.int/__data/assets/pdf_file/0004/193108/REVIHAAP-Final-technical-report-final-version.pdf?ua=1), 2013.

Whitten, G. Z., Heo, G., Kimura, Y., McDonald-Buller, E., Allen, D. T., Carter, W. P. L., and Yarwood, G.: A new condensed toluene mechanism for Carbon Bond: CB05-TU, Atmos. Environ., 44, 5346–5355, doi: 10.1016/j.atmosenv.2009.12.029, 2010.

Zhang, J., and Rao, S.T.: The role of vertical mixing in the temporal evolution of ground-level ozone concentration. J. Appl. Meteorol., 38, 1674-1690, doi: 10.1175/1520-0450(1999)038<1674:TROVMI>2.0.CO;2, 1999.

Zhang, Y., Wen, X-Y., Wang, K., Vijayaraghavan, K., and Jacobson, M.S.: Probing into regional O_3 and particulate matter pollution in the United States: 2. An examination of formation mechanisms through a process analysis technique and sensitivity study, J. Geos. Res., 114, D22305, doi: 10.1029/2009JD011900, 2009
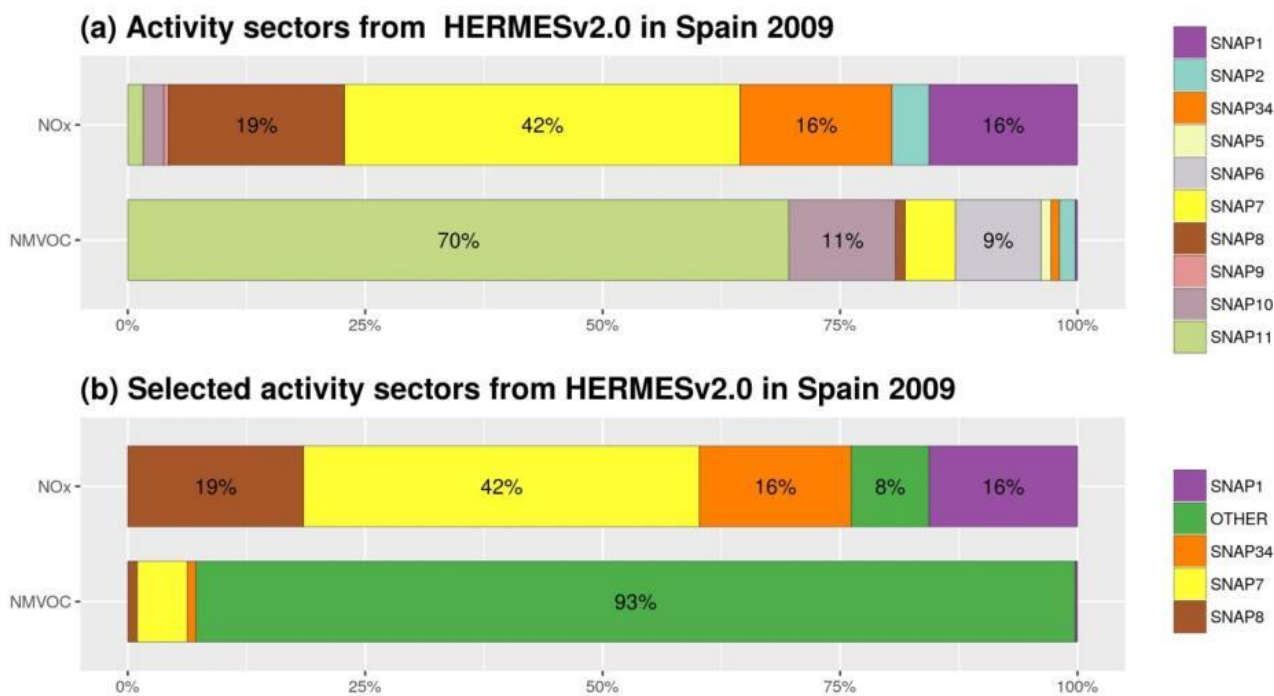
Figure 1: Percentage of the contribution of emissions to total annual emissions by SNAP sector calculated by HERMES for Spain 2009 (a) and for the selected SNAP sector accounting for more than 90% of NO_x total emission to be tracked with ISAM (b). "OTHER" compiles the SNAP categories 2 (Residential combustion), 5 (Fugitive emissions from fuels), 6 (Solvent use), 9 (Waste management), 10 (Agriculture) and 11 (Other sources).
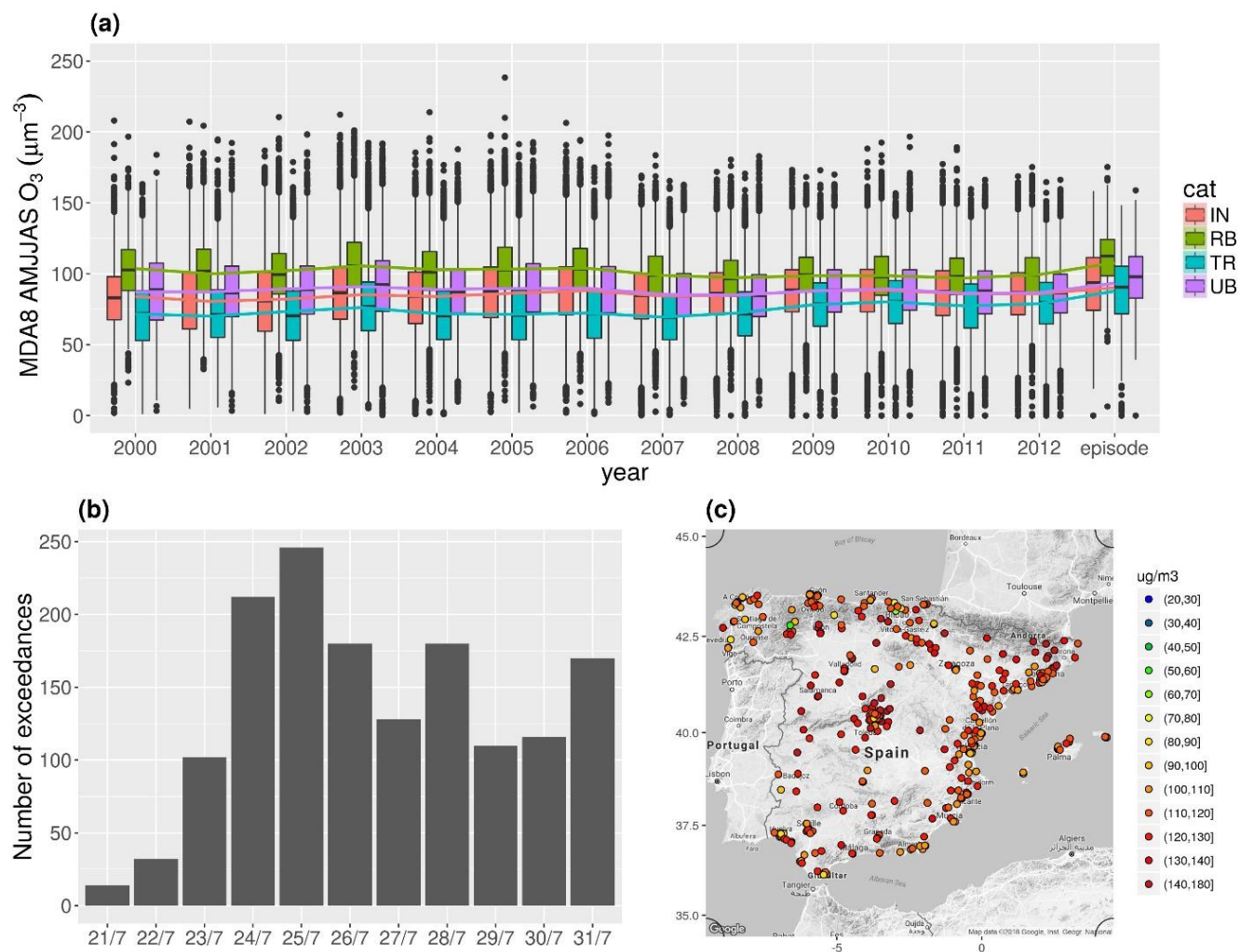
Figure 2: (a) Temporal distribution of the MDA8 O₃ concentration during the extended summer (from April to September, AMJJAS) at the Spanish EIONET stations for the period 2000-2012 and the episode (from 21/07/2012 to 31/07/2012) by station type: IN (industrial), RB (rural background), TR (traffic) and UB (urban background). (b) Number of days exceeding the O₃ Target Value (120 μg/m³) by each day of the episode. (c) 90ᵗʰ percentile of the MDA8 O₃ concentration at the Spanish EIONET stations during the episode.
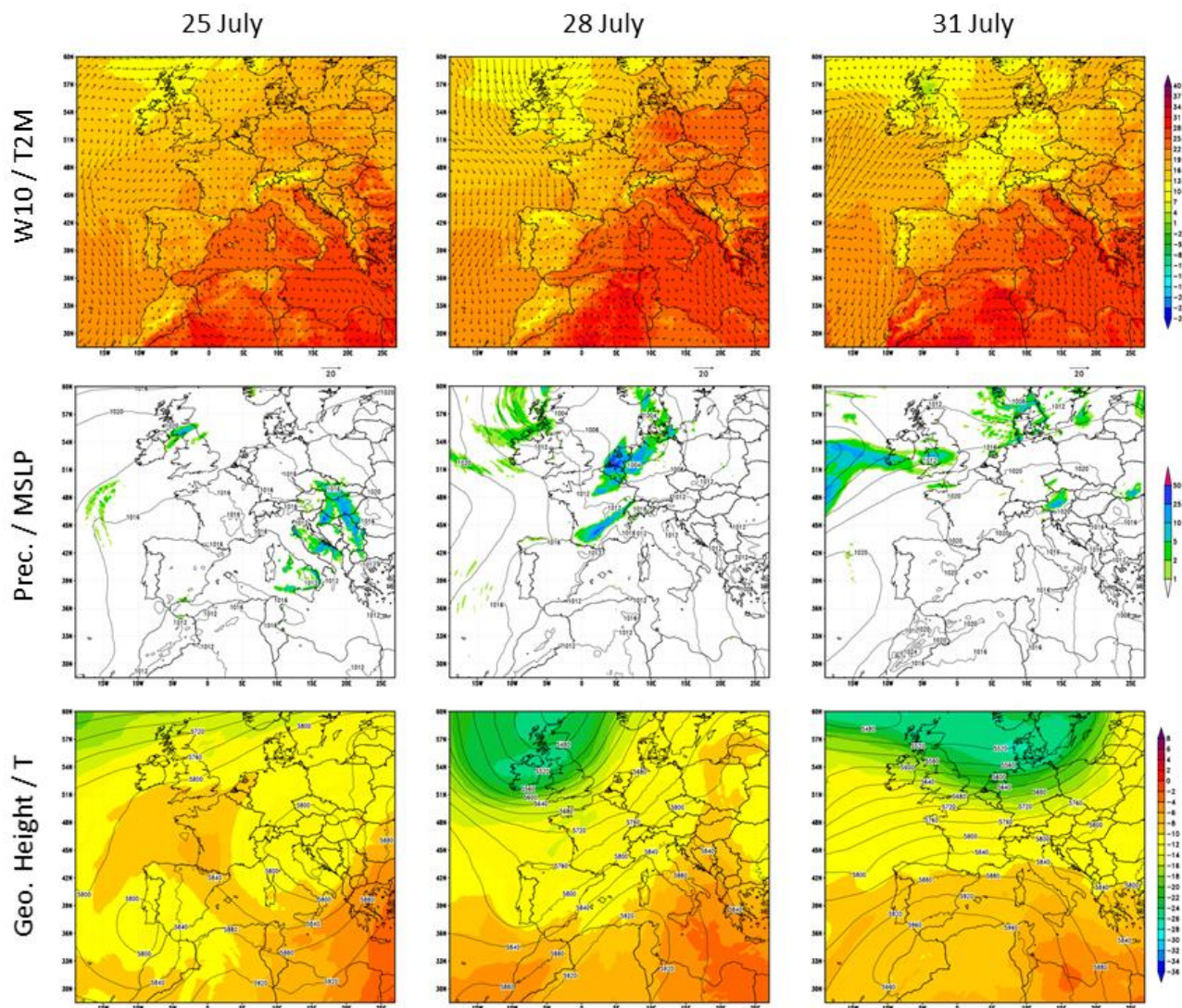
Figure 3: WRF-ARW meteorological fields at 6 UTC for July 25th, 28th and 31st in the EU12 domain: 10-m wind speed (W10, m/s), 2-m temperature (T2M, C), 6 h accumulated precipitation (Prec., mm), mean sea level pressure (MSLP, hPa), 500-hPa geopotential height in contours (Geo. Height, m), and 500-hPa temperature in shaded colors (T, ºC).
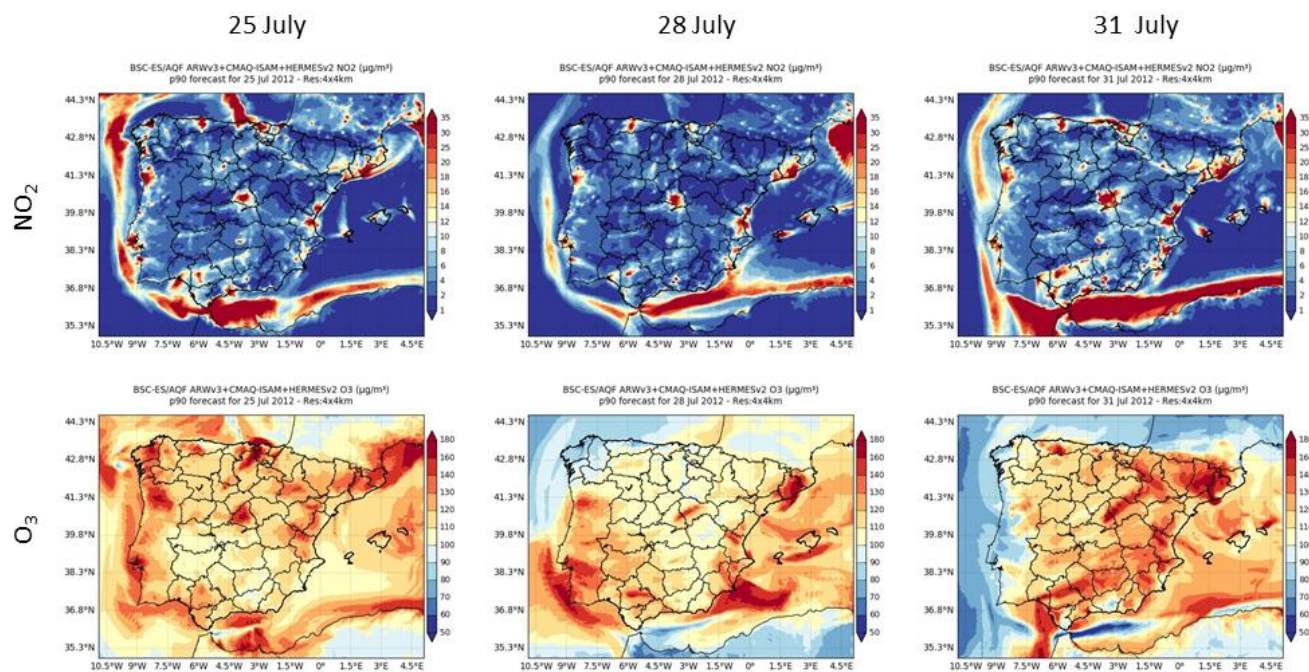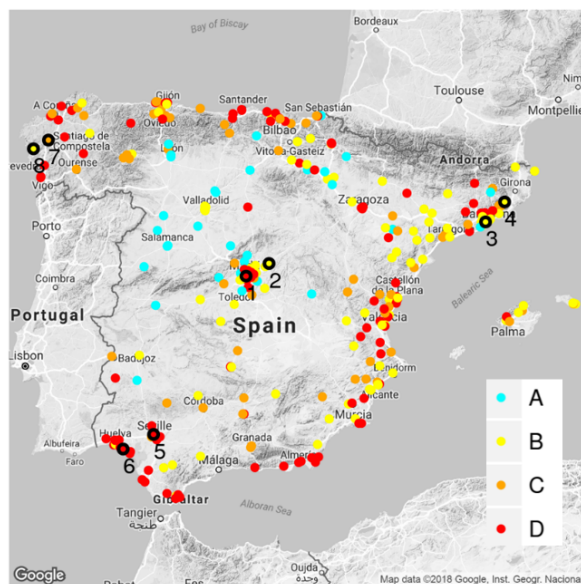
5

Figure 4: Ground-based concentration maps (in µgm⁻³) for NO₂ (first row) and O₃ (second row) corresponding to the 90th percentile of the hourly concentrations on 25th (first column), 28th (second column) and 31st (third columns) July 2012.

MB (µg/m³)		O₃ MDA8				
		<-40	(-40,-10]	(-10,10]	(10,40]	> 40
O₃ HL	<-40	0	0	0	0	0
	(-40,-10]	0	7 (2%)	0	0	0
	(-10,10]	0	A 35 (10%)	B 94 (28%)	5 (2%)	0
	(10,40]	0	3 (1%)	C 65 (19%)	D 122 (36%)	5 (2%)
	>40	0	0	0	1 (<1%)	5 (2%)

1 - CIP - D   3 - NEIP - B   5 - GV - D   7 - NWIP - D
2 - CIP - B   4 - NEIP - B   6 - GV - D   8 - NWIP - B

Figure 5: Air quality stations classified by both mean bias (MB, in µg/m³) for hourly and MDA8 O₃ at the Spanish EIONET stations and lumped by categories (A, B, C, and D). Numbered black circles indicate stations under study in Central IP (CIP; station 1 and 2), Northeastern IP (NEIP; station 3 and 4), Guadalquivir Valley (GV; station 5 6), and Northwestern IP (NWIP; station 7 and 8).
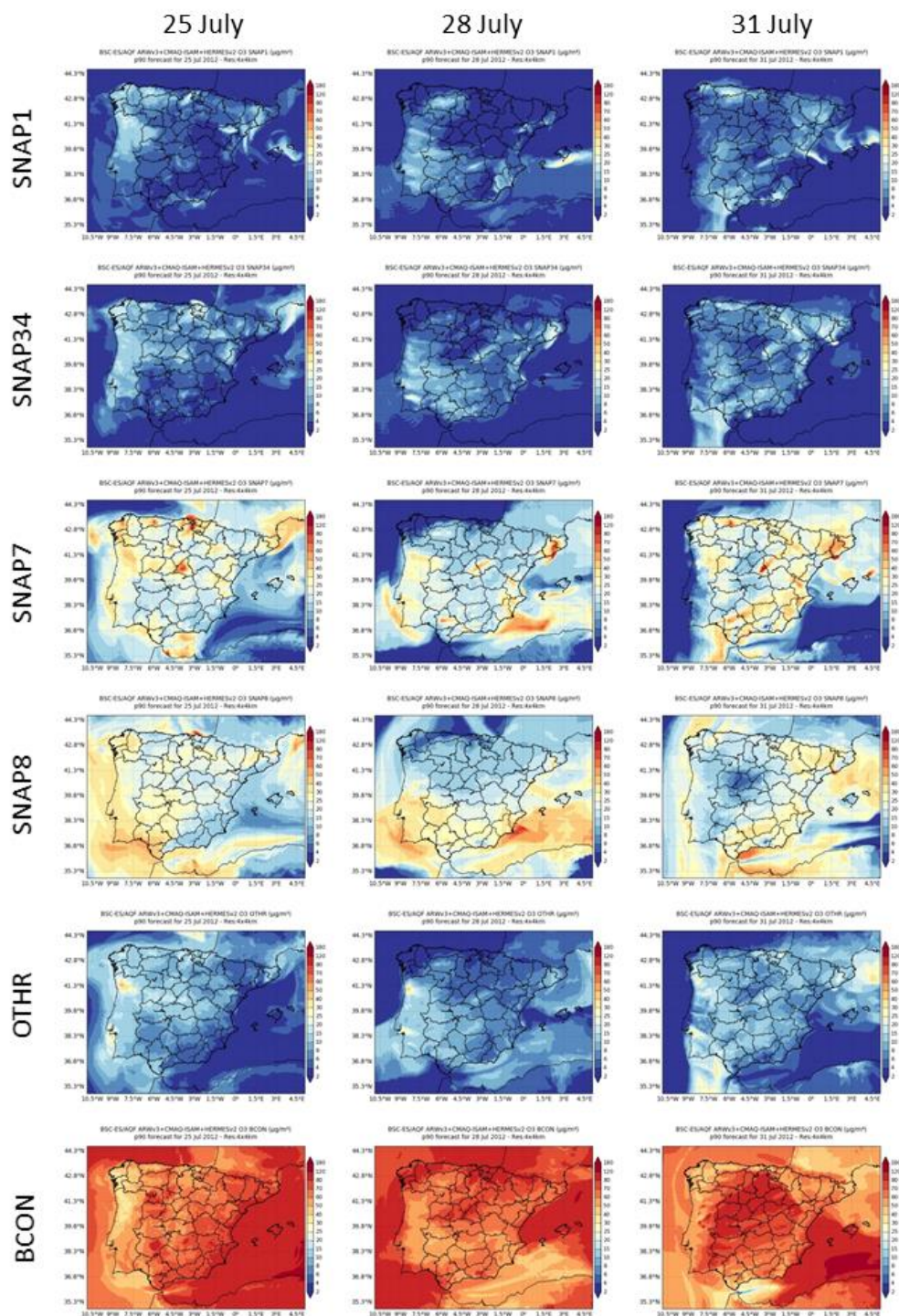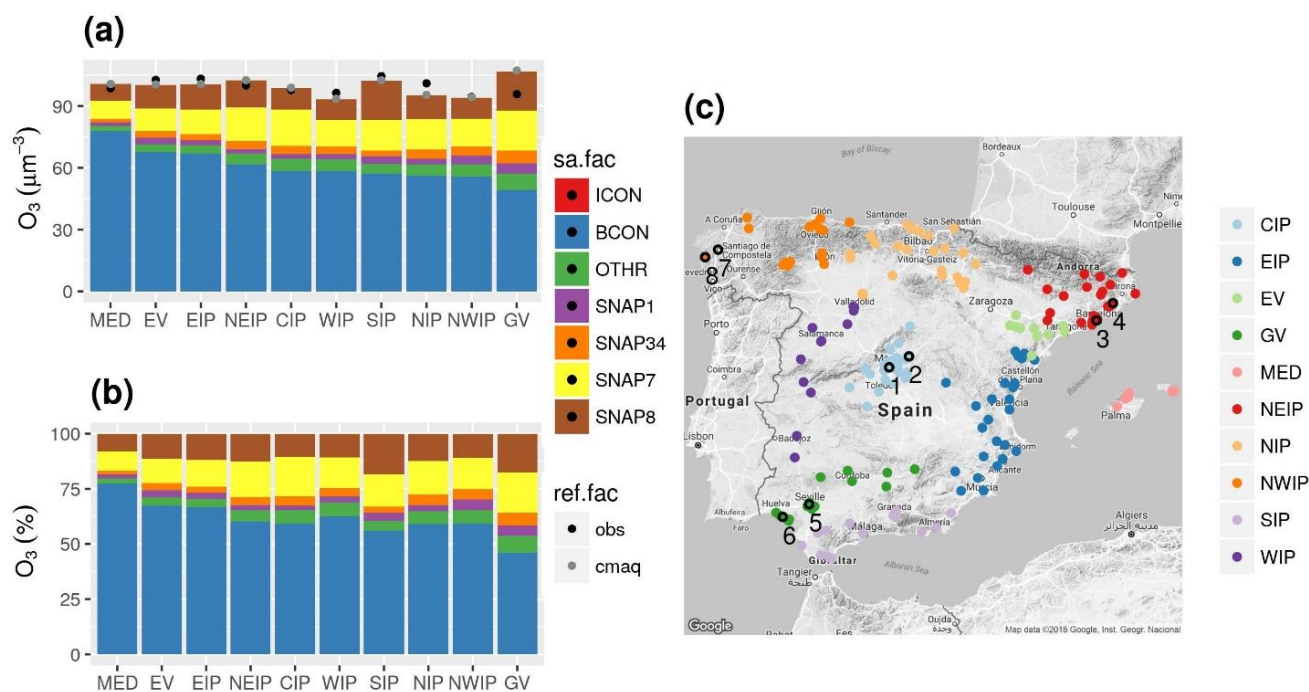
Figure 6: Tagged O₃ concentrations (in µgm⁻³) corresponding to the 90ᵗʰ percentile (90p) of the hourly concentrations: SNAP1, SNAP34, SNAP7, SNAP8, OTHER, and BCON for July 25ᵗʰ (first column), 28ᵗʰ (second column) and 31ˢᵗ (third columns) in 2012.

Atmospheric
Chemistry
and Physics
Discussions

Figure 7: Daily mean contribution in μgm⁻³ (a) and in percentage (b) of tagged sources to O₃ during exceedances of the observed 120 μgm⁻³ for MDA8 O₃ averaged by the identified receptor regions (c). Black and grey dots represent observed and modelled daily mean concentration during exceedances of 120 μgm⁻³ of the observed MDA8 O₃. Regions correspond to the Center of the IP (CIP), Eastern IP (EIP), Ebro Valley (EV), Guadalquivir Valley (GV), the Mediterranean Sea (MED), North-Eastern IP (NEIP), Northern IP (NIP), North-Western IP (NWIP), Southern IP (SIP) and Western IP (WIP). Numbered black circles indicate stations under study CI (1-2), NEIP (3-4), GV (5-6) and NWIP (7-8).

Atmospheric
Chemistry
and Physics
Discussions

Open Access
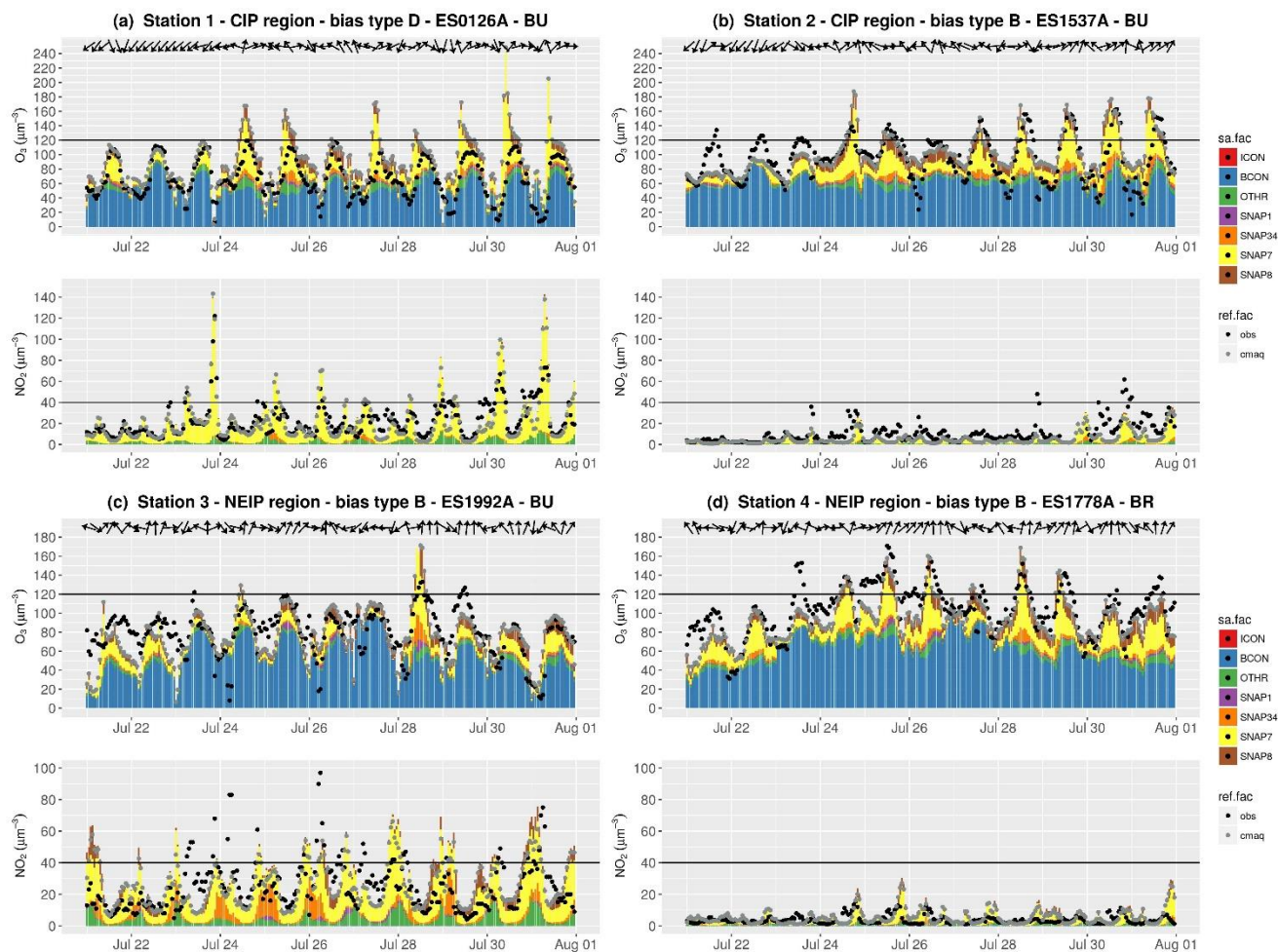
Figure 8: Source apportionment time series for O₃ and NO₂ concentrations (in µgm⁻³) in the episode at the selected stations in the Central IP (CIP) region (a,b), and in the North-Eastern IP (NEIP))(c,d). Color bars (sa.fac) indicate the O₃ tags. Black and grey dots (ref.fac) indicate the observed and modelled concentrations, respectively. Black horizontal lines represent O₃ target value (120 µgm⁻³) and NO₂ limit value (40 µgm⁻³) as a reference. The location of the stations is shown in Fig. 7 by the corresponding numbers.

Atmospheric
Chemistry
and Physics
Discussions
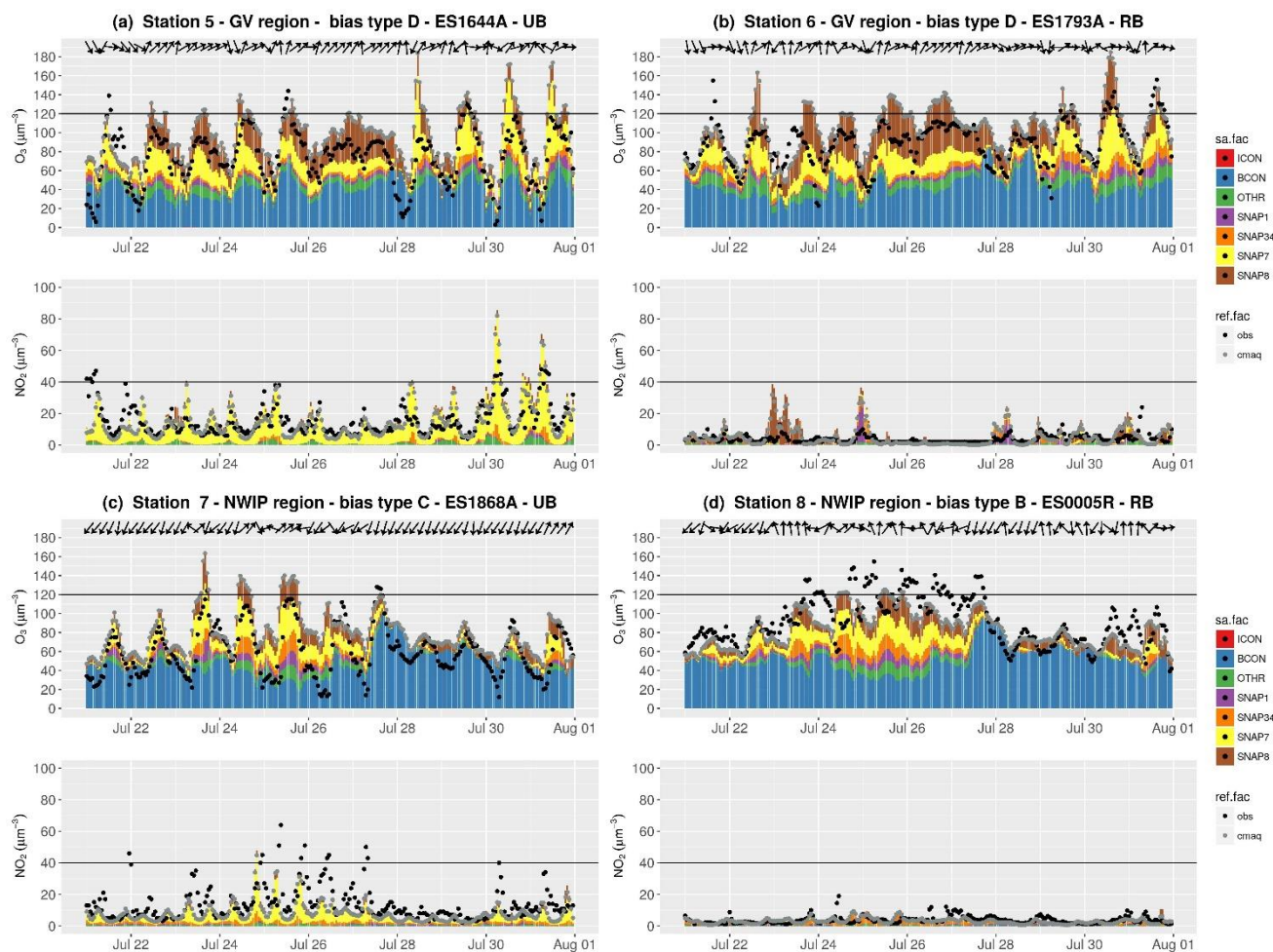
Figure 9: Source apportionment time series for O₃ and NO₂ concentrations (in µgm⁻³) in the episode at the selected stations in the Guadalquivir Valley (GV) (a,b), and in the northwestern IP (NWIP))(c,d). Color bars (sa.fac) indicate the O₃ tags. Black and grey dots (ref.fac) indicate the observed and modelled concentrations, respectively. Black horizontal lines represent O₃ target value (120 µgm⁻³) and NO₂ limit value (40 µgm⁻³) as a reference. The location of the stations is shown in Fig. 7 by the corresponding numbers.

Atmospheric
Chemistry
and Physics
Discussions
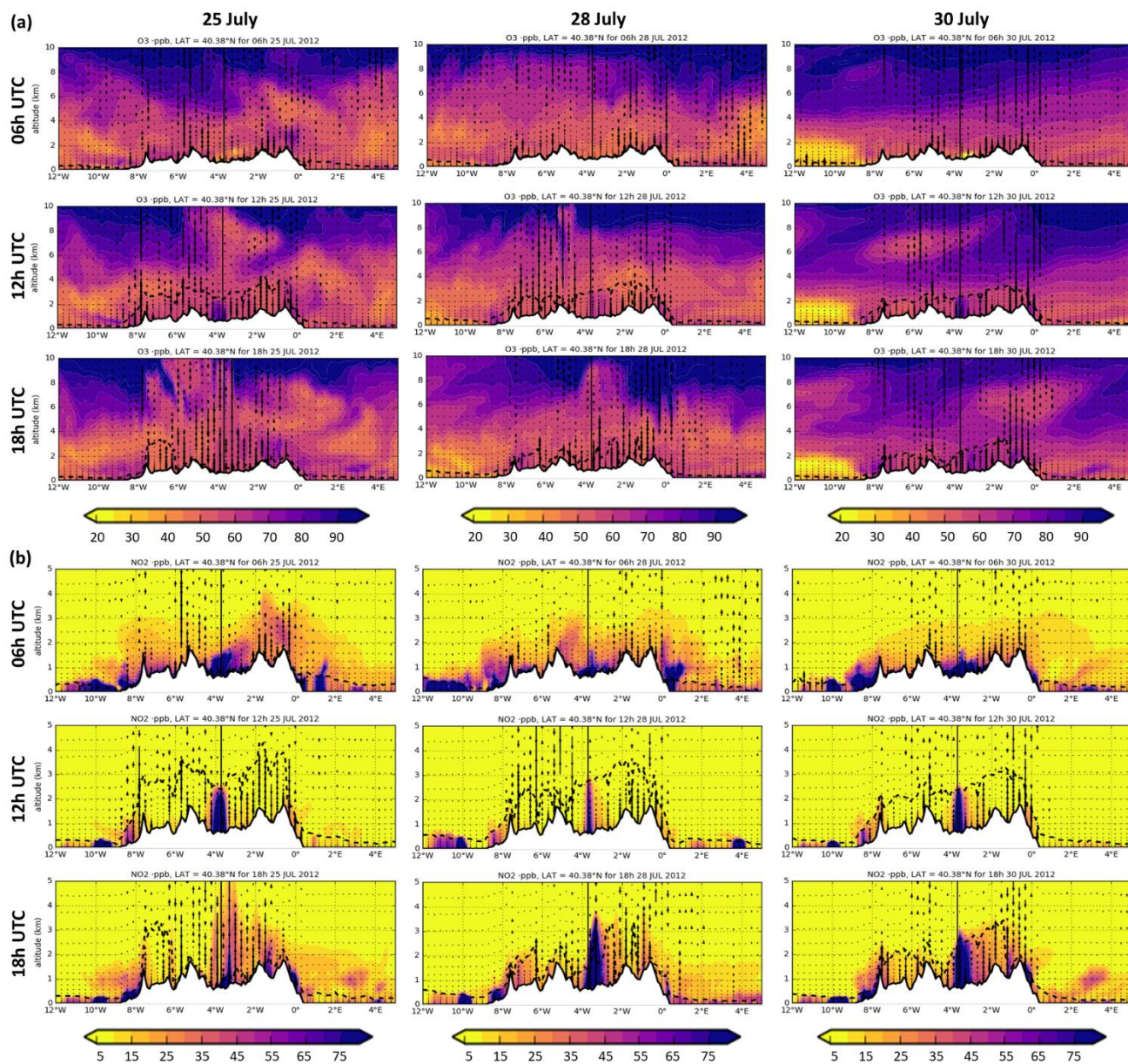
Figure 9: Cross section of modelled mixing ratios (in ppb) for O₃ (a) and NO₂ (b) at a constant latitude (Latitude = 40.38º, Madrid city) of the daily Iberian Thermal Low circulation, equivalent to the conceptual scheme of Millán et al. (1996) for July 25ᵗʰ (first column), 28ᵗʰ (second column) and 30ᵗʰ (third column) at 06, 12 and 18 UTC. Dot lines indicate the boundaries of the planetary boundary layer height. Vertical arrows indicate the vertical wind. Up arrows depict positive winds. Note the different scale for the y-axis between O₃ and NO₂.

Table 1: Description of the O$_3$ tagged sources in the present study.

ISAM tag*	Emission by SNAP category	Description
SNAP1	SNAP1	SNAP1: Energy industry
SNAP34	SNAP34	SNAP34: Industry (combustion and processes)
SNAP7	SNAP7	SNAP7: Road transport, exhaust and non-exhaust
SNAP8	SNAP8	SNAP8: Non-road transport (international shipping)
OTHR	SNAP2 + SNAP5 +	SNAP2: residential and commercial/institutional combustion
	SNAP6 + SNAP9 +	SNAP5: Fugitive emissions from fuels
	SNAP10 +	SNAP6: Product use including solvents
	SNAP11	SNAP9: waste management
		SNAP10: Agriculture
		SNAP11: Other sinks
BCON	-	Chemical boundary conditions to IP4 domain from the EU12 simulation which includes the contribution from Europe and international contribution from MOZART-4. O$_3$ external contribution
ICON	-	Initial chemical condition of the domain IP4

*Each ISAM tag is applied to O$_3$ and its precursor species in the CB05 (NO$_x$ and VOCs). NO$_x$ species contributing to O$_3$ formation involve (9 species): NO, NO$_2$, nitrogen trioxide (NO$_3$), dinitrogen pentoxide (N$_2$O$_5$), nitrous acid (HONO), peroxyacyl nitrates (PAN), higher peroxyacyl nitrates (PANX), peroxynitric acid (PNA), and organic nitrates (NTR). VOC species contributing to O$_3$ formation include (14 species): acetaldehyde (ALD2), higher aldehydes (ALDX), ethene (ETH), ethane (ETHA), ethanol (ETOH), formaldehyde (FORM), internal olefin (IOLE), isoprene (ISOP), methanol (MEOH), olefin (OLE), paraffin (PAR), monoterpene (TERP), toluene (TOL), and xylene (XYL).

5

10

Atmospheric
Chemistry
and Physics
Discussions

Table 2: Statistics for hourly O$_3$, MDA8 O$_3$, and hourly NO$_2$ concentrations in the episode as a function of the station type. Exceedances indicate the number of exceedances of the European Air Quality Directive Standards for hourly O$_3$ (180 µgm^{-3}), MDA8 O$_3$ (120 µgm^{-3}) and hourly NO$_2$ (200 µgm^{-3}). N indicates the number of monitoring stations used in the statistics calculation. MO and MM depict the measured and modelled mean concentrations, respectively. Statistics are calculated by considering more than 75 % of the hours in a day, as established by Directive 2008/50/EC. The statistics correspond to following quantiles 50th (25th, 75th) by station. Type indicates the station categories in the calculation of statistics: all the stations (ALL), industrial (IN), traffic (TR), urban background (UB) and rural background (RB) stations. Note that there are stations that do not fit in any of these four classifications.

Pollutant	Type	Exceedances	N	MO (µgm^{-3})	MM (µgm^{-3})	MB (µgm^{-3})	RMSE (µgm^{-3})	r
Hourly O$_3$	ALL	26	347	77.3 (66.7,86.5)	89.9 (83.5,95.6)	12.6 (4.4,20.2)	26.7 (21.5,32.1)	0.6 (0.6,0.7)
	IN	5	106	74.1 (62.2,83.2)	82.2 (83.4,94.5)	14.1 (4.5,21.5)	26.8 (21.1,32.8)	0.7 (0.6,0.7)
	TR	0	70	68.4 (57.1,76.7)	83.8 (74.4,89.2)	15.9 (8,21.8)	28.8 (24.5,33.9)	0.6 (0.5,0.7)
	UB	0	56	74.8 (64.1,80.0)	89.4 (81.4,94.5)	15.6 (7.8,21.3)	28.2 (24.5,33.5)	0.7 (0.6,0.7)
	RB	17	66	91.2 (80.9,97.1)	96.2 (92.6,99.6)	4.5 (-3.3,14.7)	21.2 (18.3,28.0)	0.7 (0.6,0.7)
MDA8 O$_3$	ALL	751	347	101 (91.0,113.4)	106.2 (101.8,113.2)	5.7 (-3.7,16.9)	17.9 (13.5,25.4)	0.6 (0.4,0.8)
	IN	204	106	96.7 (88.9,109.5)	104.8 (99.4,109.2)	5.7 (-2.9,16.5)	17.0 (13.0,24.5)	0.7 (0.5,0.8)
	TR	62	70	92.7 (83.6,99.9)	104.1 (98.3,110.2)	13.3 (4.6,23.8)	21.2 (15.2,31.2)	0.5 (0.3,0.8)
	UB	86	56	100.0 (89.3,105.5)	107.6 (102.2,122.8)	14.1 (2.1,21.7)	22.6 (15.6,28)	0.6 (0.3,0.8)
	RB	260	66	113.1 (104.9,119.9)	108.6 (104.5,113.2)	-3.7 (-11.1,5.5)	15 (11.8,20.2)	0.7 (0.6,0.8)
Hourly NO$_2$	ALL	3	357	14 (8.4,21.2)	9.9 (4.4,16.2)	-4.1 (-8.4,-0.5)	12.8 (8.2,17.6)	0.4 (0.3,0.6)
	IN	0	120	11.5 (7.9,16.3)	8.8 (3.8,14.7)	-3.0 (-6.6,0.2)	11.0 (7.9,15.6)	0.4 (0.3,0.5)
	TR	3	95	22.9 (17.7,28.7)	14.1 (8.7,21.6)	-7.4 (-13.9,-2.6)	18.4 (14.1,23.1)	0.4 (0.3,0.6)
	UB	0	63	17.0 (13,21.2)	13.2 (7.8,18.4)	-4.0 (-8,-0.3)	14.1 (10.5,17.3)	0.5 (0.4,0.6)
	RB	0	41	4.3 (3.5,9.3)	2.8 (1.6,4.0)	-2.0 (-5.3,-0.3)	4.4 (2.7,7.1)	0.3 (0.2,0.4)